Environmental Science and Pollution Research (2021) 28:9806–9823
https://doi.org/10.1007/s11356-020-11373-z

RESEARCH ARTICLE

Aerosol properties in the atmosphere of Natal/Brazil measured by an AERONET Sun-photometer

Daniel Camilo Fortunato dos Santos Oliveira[1] · Elena Montilla-Rosero[2] · Fábio Juliano da Silva Lopes[3,4] · Fernando Gonçalves Morais[4,5] · Eduardo Landulfo[4] · Judith Johanna Hoelzemann[6]

Received: 20 May 2020 / Accepted: 21 October 2020 / Published online: 6 November 2020

Abstract

We analyzed data measured by a Sun-photometer of the RIMA-AERONET network with the purpose to characterize the aerosol properties in the atmosphere over Natal, state capital of Rio Grande do Norte, at the coast of Northeast Brazil. Aerosol Optical Depth, Ångström Exponent, Volume Size Distribution, Single Scattering Albedo, Complex Refractive Index, Asymmetry Factor, and Precipitable Water were analyzed from August 2017 to March 2018. In addition, MODIS and CALIOP observations, local Lidar measurements, and modeled backward trajectories were analyzed in a case study on February 9, 2018, that consistently confirmed the identification of a persistent aerosol layer below 4 km agl. Aerosols present in the atmosphere of Natal showed monthly mean Aerosol Optical Depth at 500 nm below 0.15 (~ 75%), monthly means of the Ångström Exponent at 440–670 nm between 0.30 and 0.70 (~ 69%), bimodal Volume Size Distribution is dominantly coarse mode, Single Scattering Albedo at 440 nm is 0.80, Refractive Index - Real Part around 1.50, Refractive Index - Imaginary Part ranging from 0.01 to 0.04, and the Asymmetry Factor ranged from 0.73 to 0.80. The aerosol typing during the measurement period showed that atmospheric aerosol over Natal is mostly composed of mixed aerosol (58.10%), marine aerosol (34.80%), mineral dust (6.30%), and biomass burning aerosols (0.80%). Backward trajectories identified that 51% of the analyzed air masses over Natal originated from the African continent.

Keywords Sun-photometer · Aerosol · Mineral dust · AERONET · Lidar · HYSPLIT · ITCZ

Responsible Editor: Gerhard Lammel

✉ Judith Johanna Hoelzemann
judith.hoelzemann@ccet.ufrn.br

[1] Graduate Program in Climate Sciences (PPGCC), Federal University of Rio Grande do Norte (UFRN), Natal, Brazil

[2] Physical Sciences Department, School of Science, EAFIT University, Medellín, Colombia

[3] Environmental Science Department, Institute of Environmental, Chemical and Pharmaceutical Science, Federal University of São Paulo – UNIFESP, Rua São Nicolau, 210, Centro, 09913-030, Diadema, São Paulo, Brazil

[4] Center for Lasers and Applications, Nuclear and Energy Research Institute-IPEN, Av. Prof. Lineu Prestes, 2242, Cidade Universitária, São Paulo, São Paulo 05508-000, Brazil

[5] Physics Institute, University of São Paulo – USP, Rua do Matao, 1371, 05508-090, Sao Paulo, SP, Brazil

[6] Department of Atmospheric and Climate Sciences (UFRN/DCAC), Federal University of Rio Grande do Norte, Natal, Brazil

Introduction

One of the main atmospheric constituents is aerosols. These atmospheric components can influence radiative forcing, global climate, visibility (Seinfeld and Pandis 2016), human health (Fuzzi et al. 2015), cloud formation (Koren et al. 2008), precipitation, air quality (Orza and Perrone 2015), and the carbon cycle, modifying the land and ocean uptake of anthropogenic CO2 (IPCC 2018). Among the atmospheric aerosols, there is desert dust, which is an important component of biogeochemical cycles (Abouchami et al. 2013) and fertilization of the Amazon rainforest and oceans, contributing with micro- and macro-nutrients (Kaufman et al. 2006; Kumar et al. 2014).

Furthermore, aerosols are a considerable source of uncertainties in the planetary energy budget (Wang et al. 2016; IPCC 2018). A detailed knowledge of their optical and microphysical properties and distributions is required in studies of the Earth's climate and its temporal variations (Hamill et al. 2016) to reduce the uncertainties about the impact of aerosols on climate (IPCC 2013; Foyo-Moreno et al. 2019). The effects

of aerosol on the climate system can be roughly classified into three categories: (i) direct aerosol interaction with the electromagnetic radiation (direct effect – Thorsen et al. 2020). (ii) A fast feedback of the direct effect: aerosol scattering, and absorption reduce shortwave photon flux below the aerosol layer, therefore can result in cooling of the surface. Moreover, in case of absorbing aerosols, the aerosol layer gets warmer. A cooler surface and a warmer aerosol layer translate to an increase in the thermodynamic stability of the atmospheric below the aerosol layer. Such aerosol effects on the thermodynamic profiles are sometimes referred to as the semi-direct effect (Hansen et al. 1997; Koren et al. 2004). (iii) The third class of aerosol effects is related to aerosol-cloud interactions in which aerosols affect cloud properties and lifetime and thereby the planet's radiation budget (Seinfeld et al. 2016). The climate effects due to aerosol-cloud interactions are not well understood and are considered the largest source of uncertainty in climate predictions (IPCC 2018). Aerosol size distribution and properties control droplet activation and ice nucleation and therefore many of the cloud's microphysical properties are tight strongly to the dynamical ones. For example, the initial droplet size distribution will determine fluxes of latent heat and will affect buoyancy, updrafts in the cloud, and droplet mobility (Feingold et al. 2016; Koren et al. 2015). The overall effect is the result of many competing microphysical and dynamical processes and feedbacks and thus depends strongly on the type of clouds and the thermodynamic properties of the field (Seinfeld et al. 2016). To better understand the details of these interactions under different conditions, there is a need of monitoring and studying both aerosols of anthropogenic and natural origins.

The monitoring and observation of atmospheric aerosols can be performed by different remote sensing techniques. In the last decades, worldwide remote sensing networks were created to improve our knowledge on aerosols such as the WMO's Global Atmospheric Watch (GAW) (Wehrli 2000), the European Aerosol Lidar Network (EARLINET) (Pappalardo et al. 2014), the Latin American Lidar Network (LALINET) (Guerrero-Rascado et al. 2016; Antuña-Marrero et al. 2017), the NASA's Micro-Pulse Lidar Network (MPLNET) (Welton et al. 2001), the Asian Dust and Aerosol Lidar Observation Network (AD-Net) (Nishizawa et al. 2016), Network for the Detection of Atmospheric Composition Change (NDACC) (De Mazière et al. 2018), and also the Aerosol Robotic Network (AERONET) (Holben et al. 1998). The latter is focused on the effort to reduce uncertainties in the estimate of radiative forcing of aerosols (Holben et al. 1998). In addition, instruments onboard satellites such as CALIPSO (Winker et al. 2009; Omar et al. 2009), Aqua/Terra (Remer et al. 2005), EarthCARE (Illingworth et al. 2015), and Aeolus (https://www.esa.int/) have been playing an extremely relevant role in monitoring aerosols and clouds globally.

In order to study atmospheric aerosols, the Federal University of Rio Grande do Norte in Natal, Brazil, has joined the AERONET network through RIMA (*Red Ibérica de Medida fotométrica de Aerosoles*) in 2016, through a collaboration with the Institute of Energy and Nuclear Research (IPEN, São Paulo), the Research Group on Atmospheric Chemistry Modeling and Observation (GP-MOQA, UFRN), and the University of Granada (Spain). In the same year, Natal also became part of LALINET, when a ground-based Lidar was installed on the university campus in collaboration with IPEN. Natal is located in a region where the long-range transport of aerosols from the African continent frequently occurs under the strong influence of the trade winds, mostly during December, January, and February, when the Intertropical Convergence Zone (ITCZ) is positioned further to the south (Talbot et al. 1990; Swap et al. 1992; Landulfo et al. 2016; Junior et al. 2018).

Some studies show the presence of desert dust from the African continent in the atmosphere of southern hemispheric regions, such as Ascension Island (Smirnov et al. 2002), the Amazon basin (Liu et al. 2008; Ansmann et al. 2009; Ben-Ami et al. 2010; Baars et al. 2011; Baars et al. 2012; Wang et al. 2016; Moran-Zuloaga et al. 2018), and eastern Brazil (Wang et al. 2016). These studies were possible due to available observed aerosol characteristics that are required to accurately characterize the optical properties of representative types of ambient aerosol particles. Once these properties are determined, their impact on the Earth's energy budget and climate change can be assessed (Rizzo et al. 2013).

The Saharan Air Layer (SAL) has been described as a well-mixed layer with a constant potential temperature, vapor mixing ratio, and dust particles concentration with height (Karyampudi and Carlson 1988; Karyampudi et al. 1999; Berjón et al. 2019). In addition, the long-range transport of aerosol in the SAL across the Atlantic plays an important role for weather, climate, and ocean fertilization (Gasteiger et al. 2017). This layer can reach North and Central America during boreal summer (JJA) and South America during boreal winter (DJF) (Ben-Ami et al. 2012; Tsamalis et al. 2013), being modulated ITCZ (Tsamalis et al. 2013). For this reason, the SAL can play a fundamental role in transporting aerosols over Natal during the months of December, January, and February.

An important part of Saharan dust is shown to be transported within the SAL. This dust can be partly mixed with biomass burning smoke (Formenti et al. 2008; Eck et al. 2010) from December to February (Formenti et al. 2008; Weinzierl et al. 2011; Ben-Ami et al. 2012). The mineral dust is lifted to the atmosphere from many different sources and therefore, the dust composition depends heavily on the mineral content of the soil of its source region. It has been shown that Ca, K, Na, Mg, and S rich dust is linked to the Northern Sahara and Mediterranean sources, whereas Fe rich dust is linked to the Southern Sahara (Rodríguez et al. 2020).

Moreover, the presence of trace metals (Br, Cr, Ni, Zn, and Zr) is influenced by industrial emissions in North Africa (Rodríguez et al. 2020).

In this study, for the first time, a Cimel Sun-photometer was used to characterize the optical and microphysical properties of the aerosols present in the atmosphere over Natal. The paper presents the following structure: We first present the instrumentation in the "Instrumentation" section followed by the methodology (the measurement site, the description of the calculation of aerosol properties, the backward trajectories with the HYSPLIT trajectory model, and the description of other remote sensing techniques) in the "Methodology" section. In the "Results and discussion" section, we present the results and discussion of our analyses of the optical and microphysical properties as well as a case study with a Saharan dust layer, and finish with our main conclusions in the "Conclusions" section.

Instrumentation

The instrument used for the measurements in Natal is a Cimel Sun-photometer, standard model CE-318. The Cimel follows two measurement protocols, either direct Sun or sky measurements, both within several programmed sequences. The direct Sun measurements are performed in eight spectral channels (between 340 and 1020 nm, being 440, 670, 870, and 940 nm the standard channels), while sky measurements are performed at 440, 670, 870, and 1020 nm in two sky observation sequences (almucantar and principal plane) to acquire aureole and sky radiance observations across a wide range of scattering angles from the Sun through a constant aerosol profile to retrieve size distribution and phase function (Holben et al. 1998) known as inversion products (Dubovik and King 2000). The 940 nm channel retrieves the total column of water vapor or perceptible water (cm) from direct Sun measurements (Holben et al. 1998; Sinyuk et al. 2020).

To determine the spectral extinction of direct beam radiation, a filtered detector performs its measurements according to the Beer-Lambert-Bouguer law (Holben et al. 1998). Thus, the digital signal (V) measured by the instrument is proportional to the solar irradiance (Giles et al. 2019), and can therefore be expressed as an integer digital count or digital number (Giles et al. 2019) in line with Eq. (1):

$$V_\lambda = V_{0\lambda}.d^2.exp^{\left(-\tau_{\lambda total}\cdot\ m\right)} \quad (1)$$

where V_λ is the measured spectral voltage of the instrument dependent of wavelength λ, $V_{0\lambda}$ is the relative extraterrestrial spectral calibration coefficient dependent on λ, d is the ratio of the average to the present Earth-Sun distance, and m is the optical air mass which is dependent on the secant of the solar zenith angle. By these means, the total optical depth ($\tau_{\lambda total}$) is calculated and thus provides retrievals from direct Sun measurements as well as aerosol properties from inversion of spectral sky radiances (Holben et al. 1998). In addition, the optical depth is a parameter whose aerosol load is linked to the whole atmospheric column, as an indicator of the radiation attenuation by aerosol particles (Mateos et al. 2015), and the spectral dependence of the AOD is quantified by the Ångström exponent (Bennouna et al. 2011). These products allow to differentiate between different aerosol types in the atmosphere and to analyze their different optical properties (Toledano et al. 2007).

In January 2016, Natal joined the RIMA-AERONET network as the first Cimel in Natal and at the coast, and as the second in Northeastern Region of Brazil (NEB), after the AERONET station in Petrolina in the hinterlands of the state of Pernambuco, approximately 900 km from Natal. The Sun-photometers were brought to the Federal University of Rio Grande do Norte through a partnership between the Institute of Energy and Nuclear Research (IPEN, São Paulo), the Research Group on Atmospheric Chemistry Modeling and Observation (GP-MOQA, UFRN), and the University of Granada (Spain). Currently, the Cimel of Natal maintains data at level 1.5 (Table 1), i.e., data processed by AERONET algorithms and its inversion algorithm provides size distribution, refractive index, and phase function (inversion products). Additionally, along the years, the AERONET retrieval algorithm has evolved from the Version 1 algorithm based on the inversion code of Dubovik and King (2000), to Version 2 (V2) code developed by Holben et al. (2006), which improves the inversion products. Since recently, the Version 3 (V3) algorithm is being applied, which provides quality cloud scanning and fully automatic instrument anomaly quality controls (Giles et al. 2019). Level 2.0 of V2 is equivalent to the new level 1.5 of V3. The detailed descriptions about Version 3 and its processing may be found in Sinyuk et al. (2020) and Giles et al. (2019).

Methodology

Characterization of the measurement site

Natal is the capital of the state of Rio Grande do Norte located in the Northeastern Region of Brazil that comprises eight

Table 1 Cimel Sun-photometers operated in Natal labelled with AERONET numbers, start and end operation dates, numbers of days, and their product levels and versions

Identification	Start date	End date	No. of days	Level/ version
#420	29 Jan 2016	5 Jul 2016	47	2.0/V3
#752	9 Aug 2017	23 Mar 2018	102	1.5/V3

more states (Alagoas, Bahia, Ceará, Maranhão, Paraíba, Pernambuco, Piauí, and Sergipe) (Fig. 1). Natal is a coastal city (05° 47′ 42″ S, 35° 12′ 34″ W, 30 m asl) whose territory consists of sand dunes and Atlantic Forest, as well as the unique local Caatinga, a wooded savanna-like biome typical of the Northeastern region. Due to its location and regional aspect, aerosols over Natal are expected to present characteristics of biomass burning smoke, marine salt, and mineral dust. Furthermore, according to the data of the Brazilian Institute of Geography and Statistics (2020), Natal has a territorial area of 167 km^2 and an estimated population in 2019 of 884 thousand inhabitants. Furthermore, the larger Metropolitan Region of Natal is composed of 15 municipalities with a total population of 1.6 million people and a total area of 3.68 thousand km^2.

In agreement with the Brazilian National Institute of Meteorology (2017), the average temperature in Natal is 26 °C, solar irradiation produces around 3000 h of sunshine per year, and the rainfall averages to 1465 mm/year. The dry season in Natal lasts only 3 months, while the rainy season extends from January to September (Diniz and Pereira 2015), with highest rainfall during the trimester from April to June due to the Easterly Wave Disturbances (EWDs) (Motta 2004). In addition, the evaporation of the sea frequently forms very low clouds (cumulus and fractocumulus types) throughout the whole year (Motta 2004).

The climate plays a fundamental role in the characterization of aerosols because the aerosol load and composition in the atmosphere depends on both natural and anthropogenic emissions, atmospheric synoptic circulation patterns which govern long-range transport, local meteorology, and topographical characteristics (Mateos et al. 2015). In accordance with Alvares et al. (2013) who used the Köppen climate classification scheme, there are two main typical climate types in the NEB: semi-arid climate in the hinterlands as well as in parts of the states of Bahia, Piauí, and Maranhão, and tropical climate that extends along the coast from Bahia to Rio Grande do Norte (Da Silva et al. 2018). Annual rainfall of NEB is less than 500 mm/year in the semi-arid areas and three times higher (1500 mm/year) in the coastland (Reboita et al. 2010; Oliveira et al. 2016). However, the main rainy season occurs during distinct times of the year. In the hinterlands and at the northern coast, the rainfall regime takes place during the austral summer (Marengo et al. 2011; Coutinho et al. 2016;

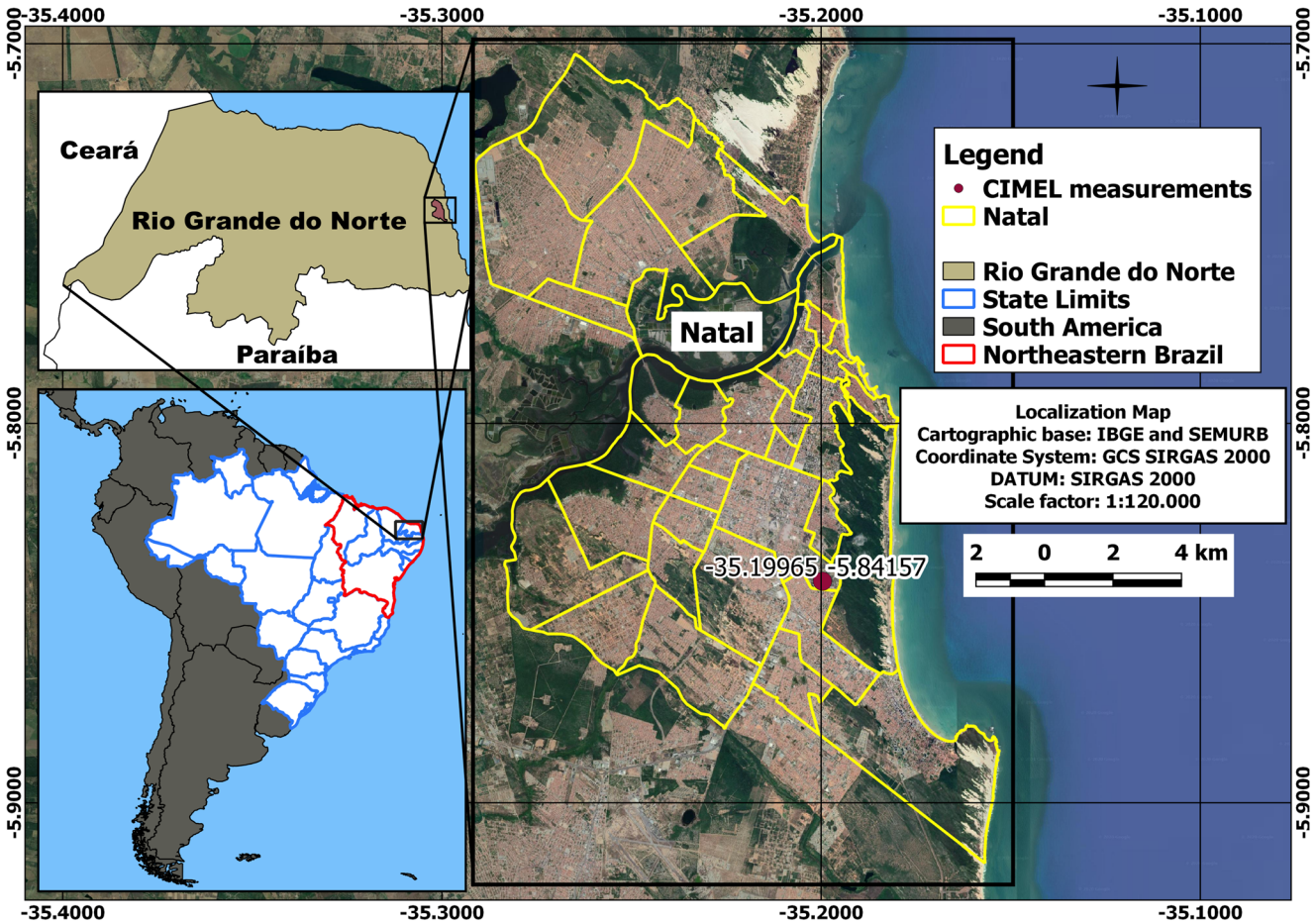

Fig. 1 Measurement site location in Northeastern Brazil (red line). The city of Natal is marked with a yellow line, and the location of the Cimel Sunphotometer is highlighted with a red dot

Reboita et al. 2016; Gomes et al. 2015), while the eastern coast's rainfall regime occurs during the austral autumn and winter (Molion and Bernardo 2002; Reboita et al. 2016).

The rainfall regime in eastern NEB is influenced by the main meteorological systems: (i) the Intertropical Convergence Zone (ITCZ) (Marengo et al. 2011; Diniz and Pereira 2015; Da Silva et al. 2018) when it is situated further south (~ 4° S) (Hastenrath 1991; Marengo et al. 2011; Reboita et al. 2016; Junior et al. 2018) during December to June (Hastenrath 1991; Melo et al. 2009), (ii) the Upper Tropospheric Cyclonic Vortex (UTCV) (Marengo et al. 2011; Da Silva et al. 2018), (iii) the sea and land breeze circulation associated with the formation of squall lines (Reboita et al. 2010; Da Silva et al. 2018) and with trade winds (Molion and Bernardo 2002), and (iv) Easterly Wave Disturbances (EWDs) (Diniz and Pereira 2015; Da Silva et al. 2018) that move westward with the trade winds associated with the subtropical ridges during the austral autumn and winter (Gomes et al. 2015).

Furthermore, in austral summer and autumn, the low-level winds of the atmosphere that reach the east coast of NEB are mostly easterly, while in austral winter and spring winds are from the southeast and more intense (Reboita et al. 2016). The land breeze comes from south, southeast, or southwest and converges with the southeast trade winds near the surface on the east coast of NEB (Diniz and Pereira 2015), forming clouds and precipitation. These wind patterns are responsible for the aerosol transportation from distant sources. All these presented phenomena favor NEB precipitation (Cavalcanti et al. 2009) and, consequently, precipitation in Natal. In contrast, another common feature of NEB is droughts. They are part of the natural climate variability in that region. They have occurred in the past, are occurring in the present and, in agreement with climate change projections, are likely to continue and intensify in the future (Marengo et al. 2016).

Calculation of aerosol properties

Aerosol Optical Depth (AOD), Ångström Exponent (AE), Single Scattering Albedo (SSA), Asymmetry Factor (AF), Refractive Index - Real Part (RIRP), Refractive Index - Imaginary Part (RIIP), and Volume Size Distribution (VSD) were the properties used in the aerosol characterization in the atmospheric column of Natal in combination with Precipitable Water (PW). These parameters were statistically and temporally analyzed from August 2017 to March 2018 (Table 1).

In this study, the wavelength 440 nm was used for the properties VSD, RIRP, SSA, RIIP, and AF with AOD (440 nm) values > 0.4 (Holben et al. 1998; Prats et al. 2008; Eck et al. 2010). For more accurate information on the aerosol type, the SSA (1020 nm) was analyzed using a similar approach to that of Foyo-Moreno et al. (2019) (difference spectral in SSA (440 nm) and SSA (1020 nm)). In addition, Derimian et al. (2008) explained that the differential aerosol spectral absorption from the blue to the near-infrared spectral region should be proportional to the associated concentrations of iron and black carbon.

The wavelength 500 nm served for the calculation of AOD, provided by AERONET with an accuracy of ~ 0.015 (Fuzzi et al. 2015). Since the mineral dust absorbs significantly in the blue and UV wavelengths, due to iron oxide impurities in the dust (Sokolik and Toon 1999; Kaufman et al. 2002; Olmo et al. 2008; Valenzuela et al. 2010), the 500 nm measurement channel is considered the standard wavelength (O'Neill et al. 2000; O'Neill et al. 2001; Smirnov et al. 2002). The range 440–870 nm was used for the AE calculation and 940 nm for PW. The AOD versus AE scatter plot is a common tool to classify aerosol types and it is the most employed classification scheme (Toledano et al. 2007; Foyo-Moreno et al. 2019). It is based on AE (440–870 nm) and AOD (500 nm) according to the main climatologies developed within the AERONET network (Eck et al. 1999; Holben et al. 2001; Smirnov et al. 2002) and it is therefore used in our analysis. Table 1 details the measurement periods for each Cimel installed in Natal, while Table 2 presents the available days with measurements and inversions at level 1.5 (V3).

HYSPLIT model

The HYbrid Single-Particle Lagrangian Integrated Trajectory (HYSPLIT) model is a complete system for computing simple air parcel trajectories, as well as complex transport, chemical transformation, deposition simulations (Stein et al. 2015), and dispersion of particulate matter such as the analysis by Galvão et al. (2016) for João Câmara city (in Rio Grande do Norte). According to Toledano et al. (2009), when analyzing the backward trajectories, the main assumption is that there is a link between the origin of the air mass, its path, and the aerosol observations at the receiving site. For this reason, it is important to know the air masses that arrive over the State of Rio Grande do Norte. James (1939) already studied two equatorial air masses over the Antlantic Ocean (North and South Atlantic Equatorial Masses) that entered through the north of South America and the coast of NEB. According to Diniz and Pereira (2015), a unified air mass between the North and South Atlantic Equatorial Masses, called Equatorial Atlantic Mass, enters the atmosphere over the state of Rio Grande do Norte. This air mass originates from the confluences of the southeast and northeast trade winds at the ITCZ (Diniz and Pereira 2015). In addition, the persistent southeast trade winds are responsible for the constant incursions of another air mass, the Atlantic Tropical Mass (Diniz and Pereira 2015) to the coast of NEB.

In order to know the origin of the air masses that arrive in Natal, we modeled their respective backward trajectories, using the HYSPLIT model version 4, model vertical velocity,

Table 2 Days with observations and days with inversions of the Cimel Sun-photometer measurements in Natal from August 2017 to March 2018, using AERONET level 1.5 (V3) data

Months	No. of days with observations	No. of days with inversions
August 2017	10	5
September 2017	9	8
October 2017	10	6
November 2017	11	4
December 2017	16	2
January 2018	15	5
February 2018	14	-
March 2018	17	-

pattern projection, and Global Data Assimilation System (GDAS 1) as the meteorological database, an operational system from the National Weather Service National Centers for Environmental Prediction. The trajectories were calculated back in time for 10 days (240 h), which is close to the 12 days of Ben-Ami et al. (2010), Landulfo et al. (2016) and Wang et al. (2016). We analyzed every day that provided AERONET 1.5 (V3), adding up to 102 days. Each day was modeled with five backward trajectories at 500, 1500, 3000, 4000, and 6000 m arrival heights above ground level (agl) at Natal (coordinates of the UFRN-CIMEL), with a frequency of 24 h for each trajectory and arrival time (20:00 UTC). These heights were selected for our analyses due to the transatlantic aerosol transport from the African continent that generally occurs around 3000 m height (Liu et al. 2008; Ansmann et al. 2009; Baars et al. 2012; Kumar et al. 2014; Orza and Perrone 2015; Wang et al. 2016; Moran-Zuloaga et al. 2018) and also to observe possible transport at other heights.

Other remote sensing techniques

In this study, the MODerate-resolution Imaging Spectroradiometer (MODIS) (Remer et al. 2005; Levy et al. 2010) aboard Terra and Aqua satellites and the Cloud-Aerosol Lidar with Orthogonal Polarization (CALIOP) (Winker et al. 2009) aboard the CALIPSO satellite were used to verify the aerosol optical properties during a 1-day case study such as AOD and aerosol subtype classification scheme from the CALIOP system. In order to complement our aerosol analysis using AOD from the Sun-photometer, the local height of aerosol layers was observed using quick-look images from the Range Corrected Signal (RCS) at 532 nm retrieved from the Lidar system installed in Natal (DUSTER Lidar). Then, Lidar qualitative data was employed in agreement to the air masses backward trajectories retrieved by HYSPLIT model.

The level 2 products of the sensors CALIOP (532 nm) (Version 4.10) and MODIS (550 nm) (Collection 6.1) were used for comparison. The horizontal resolution of the MODIS product is 10 km × 10 km, while the horizontal resolution of the CALIOP Lidar is 5 km. According to Omar et al. (2013), the differences due to the spectral variation (500 nm and 532 nm) between the two instruments (AERONET/CALIOP) may be disregarded.

These remote sensing techniques allowed an analysis of aerosol optical properties and aerosol layer heights for 1-day case study on February 9, 2018. On this day, apart from measurements of the Cimel Sun-photometer, data from the CALIOP (aerosols type and layer height) and MODIS (AOD) sensors were available, which can be considered fortunate: MODIS has a daily overpass but a minimum AOD detection threshold (0.03–0.05) (Remer et al. 2005) that eliminates many measured pixels over the NEB, while CALIOP has a sparse overpass of around every 2 weeks. Both are hampered by very frequent cloud coverage in the region (De Oliveira et al. 2019). During the period of the AERONET measurements, the MOnitoring Aerosol Long-range Transportation OVer Natal II (MOLOTOV II) campaign with the in Natal-located DUSTER Lidar was occurring, which began in December 2017 and was finished on February 26, 2018. The ground-based Lidar measurements face the same challenges with the low and dense cloud coverage in Natal as all other instruments. However, for the day of February 9, it was possible to obtain a Lidar profile. Thus, our case study focuses on an exceptional day, where we had measurements from all four instruments.

Results and discussion

Origin of air masses

The number of backward trajectories coming from the African continent to Natal (261) and the quantity arriving from other regions (249) are depicted in Fig. 2, adding up to 510 backward trajectories modeled throughout the analyzed period for five arrival heights (500, 1500, 3000, 4000, and 6000 m agl for 102 days, where observations by the Cimel Sun-photometer were also available. Trajectories originating from the African continent arrive in Natal between 1500 and 4000 m agl, mostly at around 3000 m (70), thus validating the results found in the studies for dust layers at 3000 m altitude (Holben et al. 2001; Olmo et al. 2006, 2008; Toledano et al. 2009; Ben-Ami et al. 2010; Kumar et al. 2014; Orza and Perrone 2015and Wang et al. 2016). Within the atmospheric boundary layer, at 500 m, only 22 backward trajectories reach back to the African continent, while at 6000 m height, more than the double (47) trajectories show this behavior. Trajectories from other origins show an inverse behavior: 500 m was the height with most backward trajectories originating from other directions (80), decreasing to 32 at 3000 m

height and increasing at 6000 m (55). These air masses are likely governed by the ITCZ and by the Easterly Wave Disturbances during the modeling period of the backward trajectories.

Aerosol optical properties

The measured monthly averages of AOD (500 nm) in Natal during the analyzed period ranged from 0.10 to 0.15 (Fig. 3a). These values are close to those found by Smirnov et al. (2002) for coastal areas and continental seas (AOD (500 nm) > 0.12). Probably, the low variability of AOD (500 nm) in most of those measurement months is due to the influence of local sources, such as the ocean. However, in February 2018, the AOD (500 nm) average was exceeded (0.20), that can be associated with the transport of dust and biomass burning from the African continent (DJF) (Formenti et al. 2008; Weinzierl et al. 2011; Ben-Ami et al. 2012; Tsamalis et al. 2013) in accordance with the backward trajectories (above 50% come from African continent) in the previous subsection.

The density histogram (Fig. 3b) shows that the AOD (500 nm) over Natal is dominant in the region between 0.05 and 0.15 for ~ 75% of the values, and between 0.15 and 0.20 for ~ 20% of all AOD values. Similar results were obtained by Holben et al. (2001) for Greenbelt (USA) (modal value about 0.1), for Sevilla (New Mexico) (modal value around 0.07), for HJ Andrews (Oregon) (below 0.1 for 30% during the rainy season), for Sal Island (Cape Verde) (~ 0.20 for 30% of the AOD values), for Mongu (Zambia) (maximums 0.10 to 0.20), and for Thompson (Canada) (AOD less than 0.20). The decay of the frequency density in the histogram (Fig. 3b) to values above 0.20 is represented by ~ 5% of them. In general, for Holben et al. (2001), modal AOD values lower than 0.20 are attributed to the presence of marine aerosols and AOD between 0.20 and 0.50 to desert aerosols, depending on the characteristics of the measurement site. Furthermore, an AOD lower than 0.20 can also be attributed to biomass burning aerosols (Sena and Artaxo 2015).

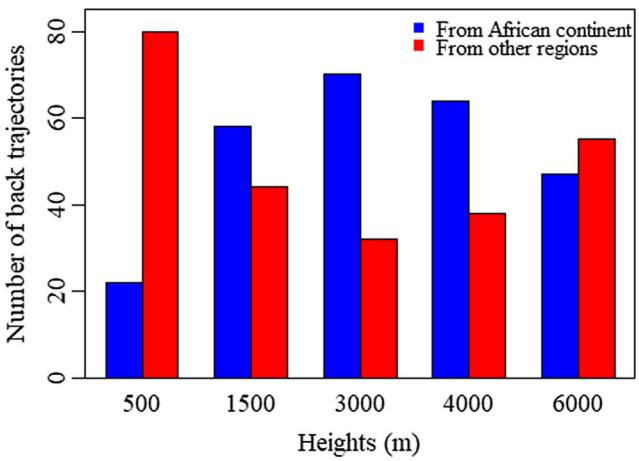

Fig. 2 Bar graph for the backward trajectories from Africa (blue color) and from other directions (red color) in five different height levels (500, 1500, 3000, 4000, and 6000 m agl) from August 2017 to March 2018

Figure 3c shows that the monthly averages of AE (440–870 nm) are between 0.30 and 0.70 for December 2017 to March 2018, the lowest monthly average being in November 2017 (0.35 ± 0.13), and the maximum monthly average in October 2017 (0.67 ± 0.19). The last value is close to those found by Holben et al. (2001) in Cuiabá (Brazil) (~ 0.60 to 0.70) during June and December 1993, and January 1994, during the nonburning season. A high variability is noticeable in December 2017, reinforcing the influence of aerosol sources associated with regional meteorology (ITCZ) in DJF (Hastenrath 1991; Melo et al. 2009; Junior et al. 2018). Although there is an AOD increase in February (Fig. 3a), the mean AE remained around 0.54 ± 0.10 for the same month and a similar behavior was found by Eck et al. (2010) in Ilorin (Nigeria) where the dust events dominated months were February through June (0.60) with a maximum AOD increase of 1.10 in January and February.

The highest AE variability during the measurement period occurred from August to December 2017. Variations in AE suggest significant variations in particle size distributions for periods of mixed aerosol size and type (Eck et al. 2005). September presents the highest concentration of AE values in the 1st quartile, while the largest amplitude (maximum and minimum values) is presented in December. The high variability of September and December may partially be the effect of high sensitivity of AE values to variations of AOD (Vergaz et al. 2005). In other words, values with very low levels of AOD can cause higher errors in the exponent (Tan et al. 2015; Foyo-Moreno et al. 2019). This has been evidenced in the study of Wagner and Silva (2008) where AE is systematically over- or underestimated depending on whether the relative error of the shorter wavelength is larger or smaller compared with the relative error of the longer wavelength. Also, the AE high variability may arise from the contribution of external sources, such as biomass burning smoke transported by the SAL-ITCZ (the "Origin of air masses" subsection) coming from the Africa continent in the biomass burning season that occurs from November through March (Eck et al. 2010). Finally, the contribution of small biomass burning activities in and around the Metropolitan Region of Natal (National Institute of Space Research 2020) may also result in varying AE. De Oliveira et al. (2019) analyzed AOD data from MODIS for NEB and found elevated AOD in September 2010 due to the contribution of biomass burning activities in the western part of NEB. Paixão (2011) showed AE monthly mean values increase during the dry season, reaching the high values in August to November due to the emission of biomass burning aerosols in, e.g., Alta Floresta, Ji Paraná, and Cuiabá. These studies corroborate with the burning season in Central Brazil that occurs from August to

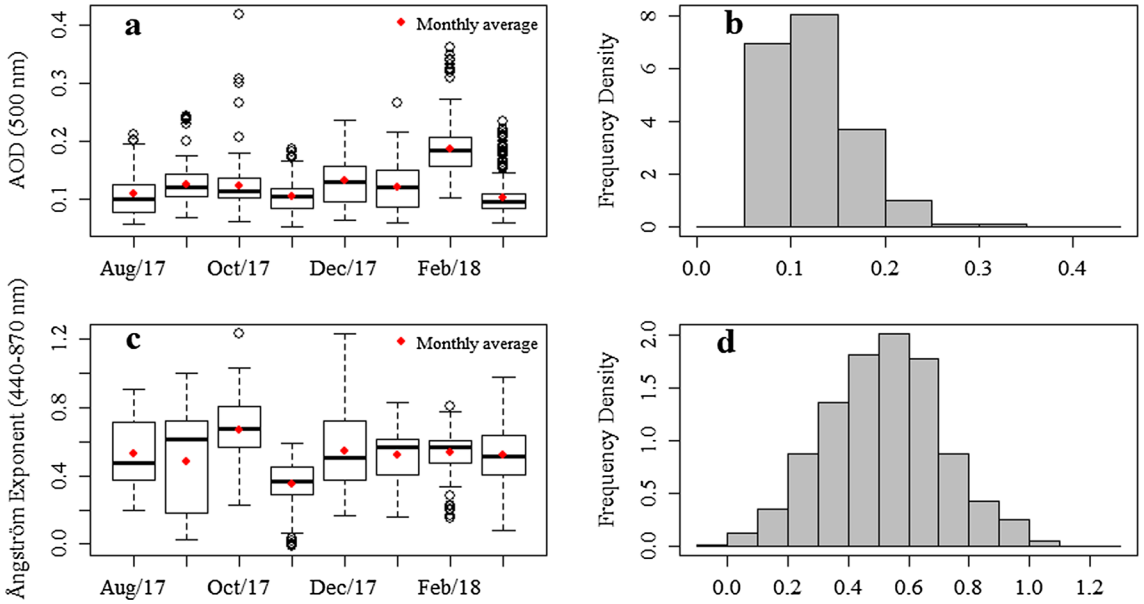

Fig. 3 Boxplots and histograms for instantaneous values of AOD (500 nm) and AE (440-870 nm) from August 2017 to March 2018 in Natal. **a** AOD (500 nm) versus months, where the base of the boxes represents the first quartile, the center lines represent the median, the top of the boxes represents the third quartile and the red dots the monthly averages. **b** Frequency density versus AOD (500 nm). **c** AE (440–870 nm) versus months, where the base of the boxes represents the first quartile, the center lines represent the median, the top represents the third quartile and the red dots are the monthly averages. **d** Frequency density versus AE (440–870 nm)

October (Hoelzemann et al. 2009; National Institute of Space Research 2020). It can be said that in general, this period is marked by high fire activity in several regions and biomes in Brazil due to different anthropogenic activities, such as deforestation, pasture maintenance, slash burn practices, and sugar cane harvesting.

The density histogram for AE (440–870 nm) (Fig. 3d) shows modal values between 0.30 and 0.70 (~ 69%). It is also relevant to highlight values between 0.70 and 1.10 (more than 20%) as they are close to the results found by Toledano et al. (2007) (mode around 1.2). The results of this optical property over Natal resemble those of Smirnov et al. (2002) for Ascension Island with dominant values typically below 1.0 (coastal sites) under scenarios with predominance of coarse particles. Expected values of marine aerosols typically have low optical depths (less than 0.15) combined with AE lesser than 1 and dust values generally have large particle sizes and high optical depths (AOD > 0.15) (Knobelspiesse et al. 2004). Therefore, AE > 1 is mainly determined by fine mode, known as submicron aerosols (Kaufman 1993), from the anthropogenic combustion sources (Eck et al. 1999), while AE < 1 is largely determined by coarse mode, known as supermicron particles (Kaufman 1993), such as desert mineral and sea salt particles (Eck et al. 1999).

Precipitable Water

The instantaneous values of PW (Fig. 4) range from 2.43 to 5.21 cm, with an increase in values from December 2017 to March 2018, which corresponds to the period of influence of the ITCZ (Hastenrath 1991; Marengo et al. 2011; Reboita et al. 2016; Junior et al. 2018). This is reinforced by the increase of the monthly average (red dots) during the observation period with a range from 3.80 ± 0.37 to 4.10 ± 0.37 cm (December to March) and, again, February 2018 stands out with a more elevated monthly average of 4.22 ± 0.48 cm. Furthermore, the east trade winds from the ocean carry humidity to the coast of NEB (Reboita et al. 2012) and the Easterly Wave Disturbances (EWDs) carry large amounts of moisture to the region (Gomes et al. 2015). The ITCZ also caused an increase of PW in the results found by Smirnov et al. (2002) during the austral summer (DJF) of Tahiti, in the results found by Holben et al. (2001) during June to September in Cape Verde and from November to December in Mongu (Zambia). The increase in Precipitable Water was also observed by Paixão (2011) during the rainy months in Brazil.

We estimated the correlation between PW and AOD (500 nm) as to 0.43. Monthly averages of AOD (500 nm) during the analyzed period remain below 0.20 (Fig. 3a), whereas the PW presents a considerable increase from December to March (Fig. 4). In Natal, the aerosol layers that result from African dust or biomass burning transport and which increase the usual AOD (550 nm) signal occur usually at 3–5 km height, far above the atmospheric boundary layer (between 280 and 1800 m agl during the rainy season, according to Da Silva 2015) and the precipitating clouds within, which does not permit to infer a direct "cause and effect" relationship between

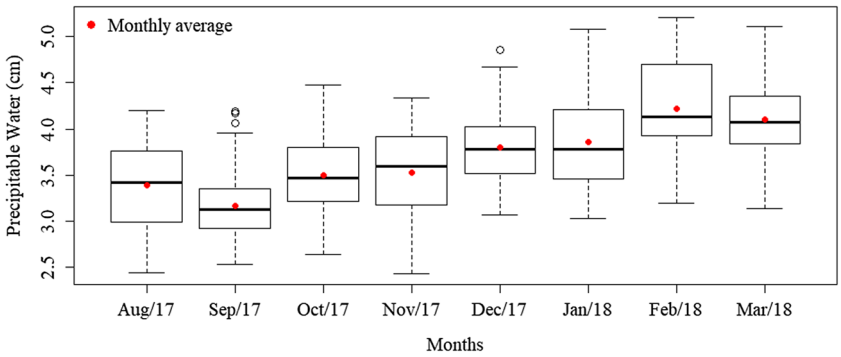

Fig. 4 Boxplots for instantaneous values of Precipitable Water (cm) each month from August 2017 to March 2018 in Natal. Red dots are the monthly averages

atmospheric PW and aerosol load. Both variables are rather driven by, and thus directly correlated to, the general meteorology of the region. A negative correlation between these two variables, due to the washout effect and wet deposition (Eck et al. 2005), is therefore not to be expected. Holben et al. (2001) considered no correlations between PW and AOD (500 nm) for Mauna Loa, Hawaii and Sal Island, Cape Verde, as well as Muyimbwa et al. (2015) who reported a correlation coefficient of 0.48 in Bergen, Norway.

Aerosol microphysical properties

Some aerosol microphysical properties retrieved from August 2017 to January 2018 are displayed in Fig. 5, Fig. 6, Fig. 7, and Fig. 8 such as SSA and AF are key parameters for the estimation of the direct radiative impact of aerosol particles (Valenzuela et al. 2010). The SSA (440 nm) remains around 0.80 for the observation period that according to Dubovik et al. (2002), Hamill et al. (2016), and Foyo-Moreno et al. (2019) is a value that is typical of particle absorption (lowest SSA) such as biomass burning smoke, urban-industrial aerosols, desert dust, and dust coated by smoke. On the other hand, the oceanic aerosol shows the highest SSA (lowest absorption). The lowest average in August (0.71 ± 0.09) (Fig. 5a) and, once again, September 2017 (0.85 ± 0.06), with the highest average, stand out suggesting the presence of biomass burning activities in the Metropolitan Region of Natal (National Institute of Space Research 2020). Similar behavior was found by Paixão (2011) for Cuiabá (0.88) during the dry season (April to September). These results are close to those found by Dubovik et al. (2002) for biomass burning in the African Savannah in Zambia (0.88 ± 0.02), by Prats et al. (2008) for a range from 0.82 to 0.97 characterized as desert dust (Huelva - Spain), and also by Foyo-Moreno et al. (2019) for SSA values of ~ 0.80 (Huelva - Spain) and ~ 0.81 (Granada - Spain) that were explained by contribution of carbonaceous species in pollution events. Our results are also comparable to those of Giles et al. (2012) for mixed aerosol SSA (0.86 and 0.87) and biomass burning SSA (0.85 and 0.87).

September also shows SSA values close to 1.0 (outliers) referring to non-absorbing aerosols (Foyo-Moreno et al. 2019), e.g., marine particles. This feature is expected for water-soluble aerosol (Dubovik et al. 2002) because the absorption may be influenced by moisture content, relative humidity (Dubovik et al. 2002), and aging during transport (Valenzuela et al. 2010). However, the SSA (440 nm) for other months is quite low, probably due to the inversions only for AOD (440 nm) > 0.4.

In general, this microphysical property points to biomass burning and mineral dust aerosols for the measurement period in Natal. Positive values of SSA (440 nm)-SSA (1020 nm) are typical of anthropogenic pollution and biomass burning, while negative SSA (440 nm)-SSA (1020 nm) are typical of dust particles (Dubovik et al. 2002; Foyo-Moreno et al. 2019). Figure 5b shows negatives values in some months, which also suggests the presence of mineral dust over Natal likely locally transported from the sand dunes during the period of more elevated wind intensity from August to October.

The AF is indicative of the rate of radiation scattered forward and is related to the particle size (Valenzuela et al. 2010). For the observation period, AF (Fig. 6) also did not change significantly and ranged between 0.73 and 0.80, with a maximum that occurs in November 2017 (0.78 ± 0.04) and the minimum occurring in October 2017 (0.74 ± 0.04). From August 2017 to October 2017, there is a slight decay with the biggest uncertainties in September (0.76 ± 0.05) and from November 2017 to January 2018, the monthly averages remain around 0.76; thus, these ranges are an indicative of predominance of coarse mode aerosols. These values agree with those of Dubovik et al. (2002) for desert dust and oceanic aerosol found in Cape Verde and Lanai (Hawaii) (0.73 ± 0.04 and 0.75 ± 0.04, respectively), as well as Taylor et al. (2015) who found values of 0.74 for mineral dust.

The Refractive Index - Real Part (Fig. 7a) remains around 1.50 with the lowest average in December 2017 (1.44 ± 0.03) and the highest average in August 2017 (1.53 ± 0.06). The Refractive Index - Imaginary Part (Fig. 7b) is variable over the measurement period, with a monthly maximum in August 2017 (0.05 ± 0.03) and the minimum in November 2017 (0.01 ± 0.01). However, there are no indications of a relation

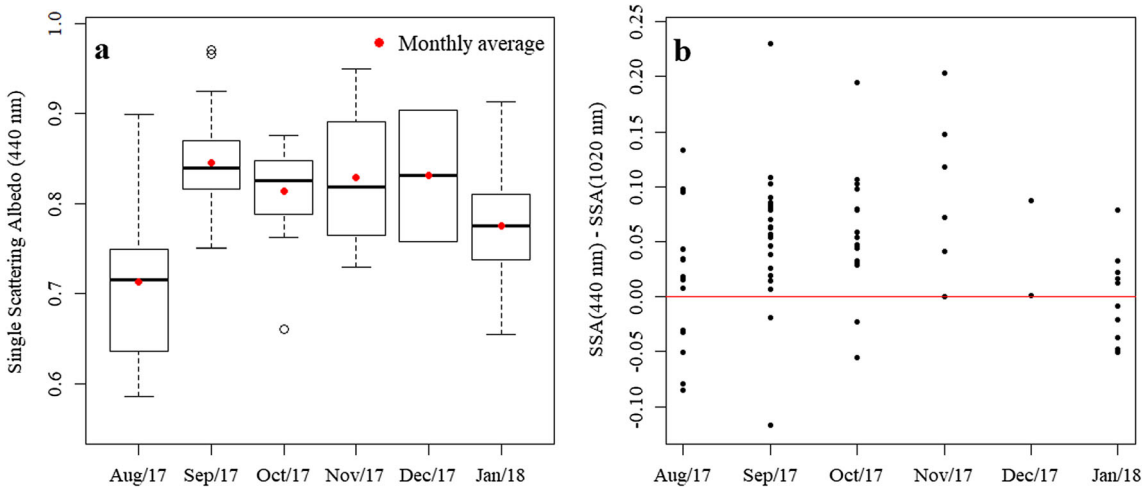

Fig. 5 **a** Boxplots for instantaneous values of Single Scattering Albedo (440 nm) versus months, where the red dots are the monthly averages. **b** Scatter plot for instantaneous values of spectral difference in SSA (440–1020 nm) for each month. Both charts are of the same period from August 2017 to January 2018 in Natal

to biomass burning, as this aerosol type is strongly absorbent (Kaufman et al. 2002). The observations of the RIRP and RIIP, respectively, are similar to those found by Dubovik et al. (2002): for mixed and industrial urban aerosol in Greenbelt (USA) (RIRP = 1.47 ± 0.03, RIIP = 0.01 ± 0.00), for biomass burning in the Brazilian Cerrado (RIRP = 1.52 ± 0.01, RIIP = 0.02 ± 0.00) and in the African Savannah (Zambia) (1.51 ± 0.01, 0.02 ± 0.00), and for desert and oceanic dust in Bahrain (Persian Gulf), Solar (Saudi Arabia), and Cape Verde (1.55 ± 0.03, 1.56 ± 0.03 and 1.48 ± 0.05, for the RIRP, respectively). Also, Perrone et al. (2005) classified the days with values of 1.46 ± 0.09 and 1.50 ± 0.07 (real part) as urban industrial aerosols in Lecce (Italy). Additionally, the dust particles are moderately absorbent with values of the RIIP from 0.005 to 0.05 (Perrone et al. 2005). This shows that the observations for Natal related to the RIIP (0.01 ± 0.01 to 0.04 ± 0.03) suggest moderately absorbent particles for our dataset.

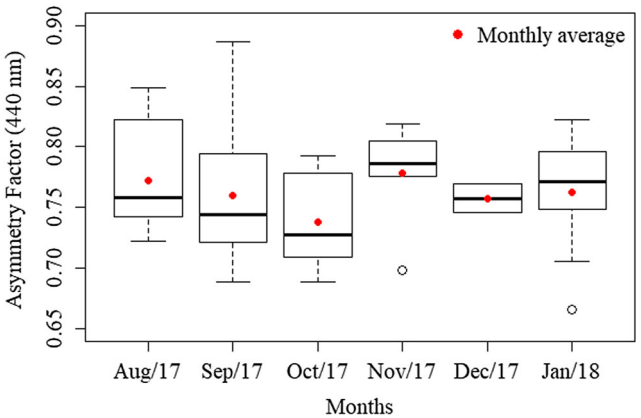

Fig. 6 Boxplots for instantaneous values of the Asymmetry Factor versus months from August 2017 to January 2018 in Natal, where the red dots are the monthly averages

All of these aerosol properties (Fig. 5, Fig. 6, and Fig. 7) remain without significant variations and do not have a strong relationship with the rainy months in Natal, suggesting that they are more linked to the internal and external sources of aerosols. Nevertheless, there is a clear link between these microphysical properties and coarse mode aerosols (marine aerosol and mineral dust).

The VSD over Natal is bimodal (Fig. 8) with a dominant volume in the coarse mode, related to the local sources such as the sea, the sand dunes, and the external sources (Africa continent). The value of the coarse mode is shown (0.02 ± 0.01 $\mu m^3/\mu m^2$) with a radius of 2.94 μm and the fine mode stands out (0.004 ± 0.002 $\mu m^3/\mu m^2$) with a radius of 0.19 μm. The radius that separates coarse mode and fine mode is 0.33 μm which is close to those found by Smirnov et al. (2002) at five islands around the globe (0.40 μm); by Taylor et al. (2015) for the dust cluster (0.35 μm); and by Foyo-Moreno et al. (2019) (between 0.4 and 0.5 μm) for seven locations of the different AERONET stations. For Giles et al. (2012), the fine mode particles have a radius < 1.0 μm in the volume size distribution, typically combustion-produced particles (Eck et al. 2010), while mixtures composed of natural aerosols (radius > 1 μm) are predominately coarse mode particles (Eck et al. 2010). The effective radius is a VSD-derived parameter which describes the aerosol size as the single-scattering properties of the size distribution are more related to the effective radius (Hansen and Travis 1974). For the coarse mode, the effective radius is 1.97 ± 0.26 μm and ranges from 1.58 to 2.99 μm from August 2017 to January 2018, while the fine mode is 0.16 ± 0.03 μm ranging from 0.12 to 0.26 μm for the same period. The low uncertainties in the effective radius can be related to a constancy in the aerosol type of the fine mode through the observation period, whereas the high uncertainty of the coarse mode can refer to different aerosol types. Similar

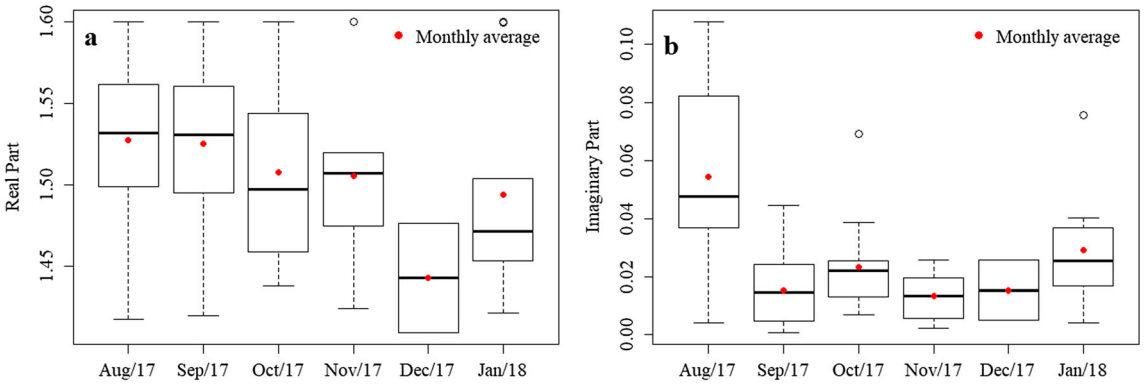

Fig. 7 Boxplots for instantaneous values of the Refractive Index from August 2017 to January 2018 in Natal. Red dots are the monthly averages. **a** Real Part versus months. **b** Imaginary Part versus months

results were found by Prats et al. (2008) (0.14 ± 0.02 μm for fine mode and 1.96 ± 0.41 μm for coarse mode) in El Arenosillo (Spanish Atlantic coast).

The greatest uncertainties are present in coarse mode mainly in the VSD tail (radii values > 4 μm) can be associated to the coarse aerosols such as maritime aerosol that interact with intense winds from the east and southeast NEB coast, mineral dust (local from dunes and remotely from African continent), or even the particle sizes that interact with the humidity brought by the land breeze and southeast trade winds near the surface, forming clouds, and precipitation (Diniz and Pereira 2015). Additionally, the large particles of mineral dust (100 μm in diameter) are found in the regions of their origin and the particles predominantly smaller than 10 μm are transported over long distances (Seinfeld and Pandis 2016).

Aerosol typing

Figure 9 provides the aerosol typing in the atmosphere over Natal from August 2017 to March 2018. It is expected that aerosol typing determines predominantly marine aerosols. The AOD instantaneous values associated with its respective AE instantaneous values classify the aerosols within ranges based on the climatologies by Holben et al. (2001) and Smirnov et al. (2002): (i) mixed aerosol consisting of mineral dust and marine aerosol and likely biomass burning (Formenti et al. 2008; Eck et al. 2010). This means that this mixed aerosol type is classified in an intermediate range between the characteristics of both mineral dust and marine aerosol, representing 58.10% of the total; (ii) marine aerosol (34.80%) originated from sea salt; (iii) mineral dust (6.30%) originated from soil (from local sand dunes and from African continent); and (iv) biomass burning (0.8%) originated from both local and remote sources (the "Origin of air masses" and "Aerosol optical properties" subsections). The high percentage of mixed aerosol is related to the challenge in distinguishing sea salt aerosols from those of dust, since both are associated with low Ångström exponents (Holben et al. 2001). Other characteristics of marine aerosols are low optical load, low AE, and high SSA (low absorption, values close to 1) (Dubovik et al. 2002) as shown in Fig. 5a.

The AOD (500 nm) averages of aerosol typing are 0.08 ± 0.01 for marine aerosol, 0.14 ± 0.03 for mixed aerosol, 0.23 ± 0.04 for mineral dust, and 0.17 ± 0.07 for biomass burning. The AE (440–870 nm) averages are 0.51 ± 0.17 (marine aerosol), 0.51 ± 0.20 (mixed aerosol), 0.54 ± 0.17 (mineral dust),

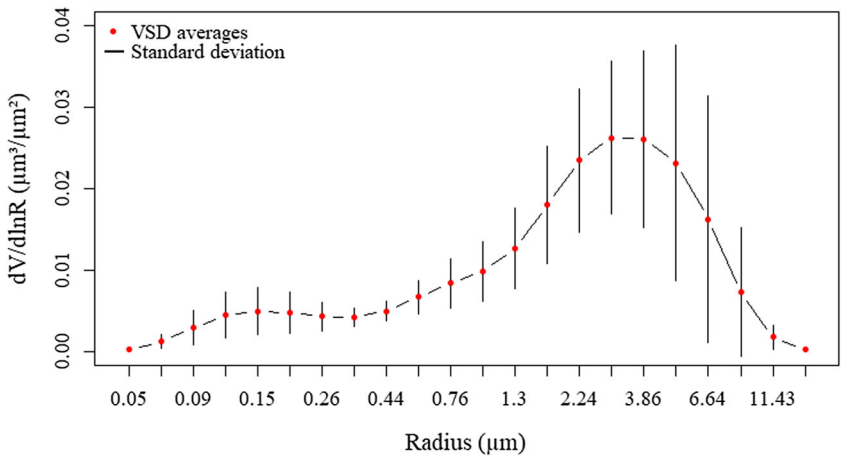

Fig. 8 Volume Size Distribution averages for instantaneous values ($\mu m^3/\mu m^2$) and respective radii (in μm) for the period from August 2017 to January 2018 at Natal by Cimel Sun-photometer, where red dots are the averages and black bars are the standard deviations

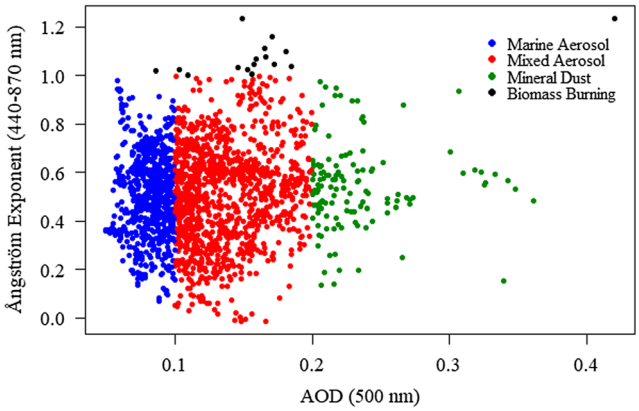

Fig. 9 Scatter plot for instantaneous values of Aerosol Optical Depth (500 nm) versus Ångström Exponent (440–870 nm) in Natal from August 2017 to March 2018. Colors indicate different aerosol types: blue (marine aerosols), red (mixed aerosols), green (mineral dust), and black (biomass burning)

and 1.08 ± 0.07 (biomass burning). It is possible to see that AE averages are predominantly around 0.50, meaning AE values over Natal are considered to be mostly coarse mode (AE < 1). These data are compatible with those found by Knobelspiesse et al. (2004) for AOD (500 nm) in North America (dust: 0.17, marine: 0.08), in the Pacific (marine: 0.09), and in South Asia, where values for marine aerosol were in the range of mixed aerosol (0.14).

Over the whole measurement period, there are instantaneous values of aerosols classified as mineral dust; however, the mineral dust predominance occurs during February 2018 (11 days) followed by December, January, and March (3 days during each month), possibly because the ITCZ is at its southernmost position during this period (DJFM), facilitating the arrival of Saharan dust over the region (Melo et al. 2009; Reboita et al. 2012; Junior et al. 2018). Thus, the location of the ITCZ can be a good indicator of the dust meteorology (Ben-Ami et al. 2012). In Fig. 3a, February 2018 also has the higher AOD for the period. Biomass burning aerosols are present in October (during 4 days) and December (during 3 days), coinciding with the burning periods in Africa (Formenti et al. 2008; Weinzierl et al. 2011; Baars et al. 2012; Ben-Ami et al. 2012) and in the Metropolitan Region of Natal (National Institute of Space Research 2020). Those classified as mixed and marine aerosols are present throughout the whole data collection period.

Case study

In accordance with the performed analysis, February 2018 (Fig. 3a and 3c) includes 11 days with aerosols classified as mineral dust, without the strong influence of the marine aerosol, i.e., this month presents the highest number of occurrences of this aerosol typing followed by December, January, and March, each month with 3 days of mineral dust classification. Two atypical days in February 2018 stood out, according to the outliers of Fig. 3a and 3c (days 9 and 28). We chose February 9 for our case study since it is the only day with overpasses of MODIS and CALIPSO satellites, as well as a short measurement of the DUSTER Lidar for terms of intercomparison.

The aerosol typing of February 9, 2018, specifies mineral dust for all observations of this day with AOD (500 nm) ranging from 0.30 to 0.37 and AE (440-870 nm) between 0.45 and 0.65. MODIS detected AOD between 0.30 and 0.45 at the coast of Rio Grande do Norte where Natal is located (Fig. 10). The CALIPSO overpass (Fig. 11) classified the aerosols near Natal as marine aerosol, dust, and dusty-marine mixed aerosols as described by Kim et al. (2018) for aerosol subtype by CALIOP. These are the most predominant aerosol subtypes provided by CALIOP Version 4.10. Thus, the MODIS and CALIOP sensors are completely in line with the Cimel Sun-photometer classification for February 9, 2018.

The backward trajectories modeled for February 9, 2018 (Fig. 12) show that the air parcels at 3000 and 4000 m above Natal origin from Central Africa and Nigeria where part of the Sahel region is located (northern Nigeria). The air masses at 3000 and 4000 m are the result of an ITCZ located further south (~ 4° S) (Hastenrath 1991; Marengo et al. 2011; Reboita et al. 2016; Junior et al. 2018). These backward trajectories fit the findings of Wang et al. (2016) who found that more than half of the dust in Central America and northern South America was coming from northwestern Sahara, followed by the contribution of the western Sahel (20–30%). Also, the authors found that the high sensitivity to emissions from the Bodélé depression is limited to the east of Brazil during the months of January 2014 to April 2014.

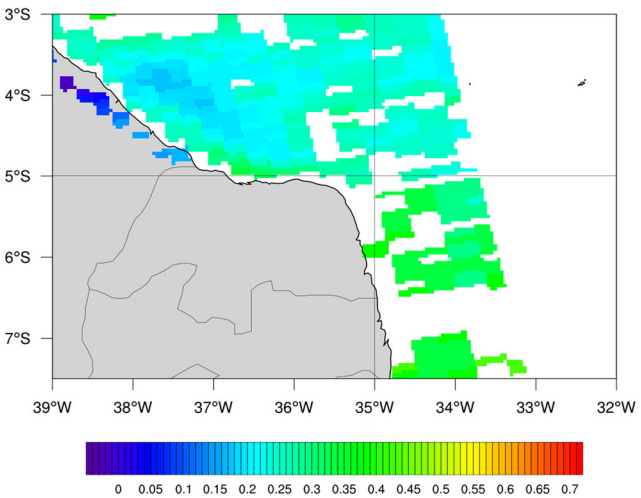

Fig. 10 MODIS daily average AOD at 550 nm derived from Aqua and Terra satellites, Level 2, Collection 6.1, and 10 km × 10 km resolution on February 9, 2018, at the coast of Rio Grande do Norte

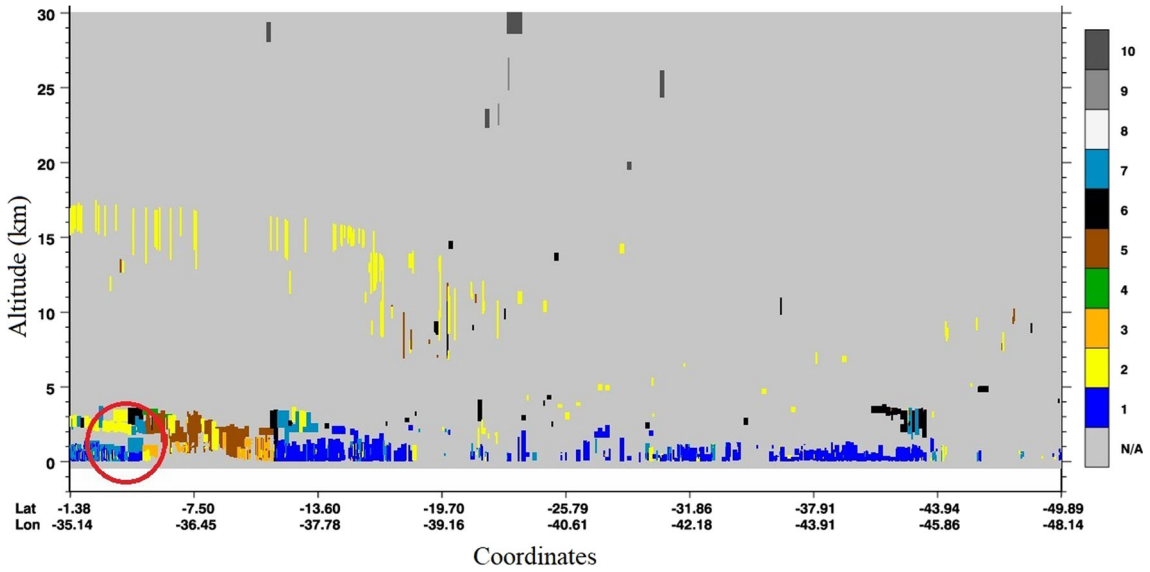

Fig. 11 Aerosol subtype observed by CALIOP, Version 4.10, Level 2 products, vertical resolution of 5 km, from 4:04 to 4:18 UTC on February 9, 2018. The closest region to Natal is highlighted with a red circle, the color bar represents the subtypes of aerosols: 1-marine, 2-dust, 3-polluted continental/smoke, 4-clean continental, 5-polluted dust, 6-elevated smoke, 7-dusty marine, 8-polar stratospheric cloud aerosol, 9-volcanic ash, 10-sulfate/other (numbers 6, 8, 9, and 10 by Kim et al. 2018), and N/A-not applicable, available on https://www-calipso.larc.nasa.gov/products

Since the HYSPLIT backward trajectories for February 9, 2018, display aerosol air masses reaching Natal at 3000 and 4000 m, we used our local ground-based DUSTER Lidar quick-look image generated by the Range Corrected Signal (RCS) at 532 nm to identify the altitude of the aerosol layer for this case. Figure 13 presents the temporal evolution of the aerosol particles suspended in the atmosphere by RCS at 532 nm retrieved by DUSTER Lidar, which is the sum of particle and molecular backscatter signal corrected by the square distance for the wavelength of 532 nm. In Fig. 13, it is possible to identify some aerosol layers below 4000 m height, which are in agreement with aerosol layers detected at 3000 m by the CALIOP system (Fig. 11), and with the air mass backward trajectories coming from the African continent at the same height is as strong indication of the transcontinental transport of aerosol layers from Africa to South America (Liu et al. 2008; Ansmann et al. 2009; Baars et al. 2012; Ben-Ami et al. 2010; Kumar et al. 2014; Orza and Perrone 2015; Wang et al. 2016; Moran-Zuloaga et al. 2018).

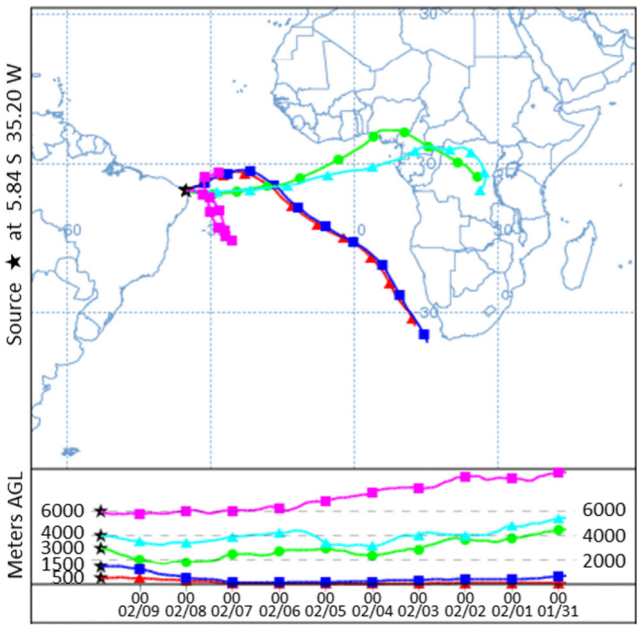

Fig. 12 Backward trajectories finalized at 20:00 UTC on February 9, 2018, based on GDAS meteorological data, HYSPLIT Model Version 4, Revision 515 and calculated by the AERONET Data Synergy Tool, available at https://aeronet.gsfc.nasa.gov/cgi-bin/bamgomas_interactive

Conclusions

For the first time, the optical and microphysical properties in the atmospheric column of Natal, Brazil, were characterized by a Cimel Sun-photometer of AERONET V3, level 1.5 observations from August 2017 to March 2018. We also have verified the data of Cimel Sun-photometer, local Lidar measurements, backward trajectories, and satellites Aqua/Terra and CALIPSO for a case study on February 09, 2018.

Most of the AOD (500 nm) values remained below 0.15 (~ 75%) and held characteristics of marine aerosol. The aerosol load increased in February 2018 which could be attributed to the intrusion of dust and biomass burning from local and remote sources. All monthly averages for AE (440–870 nm) remained between 0.30 and 0.70 (69%) from December 2017 to March 2018, meaning that aerosols over Natal are

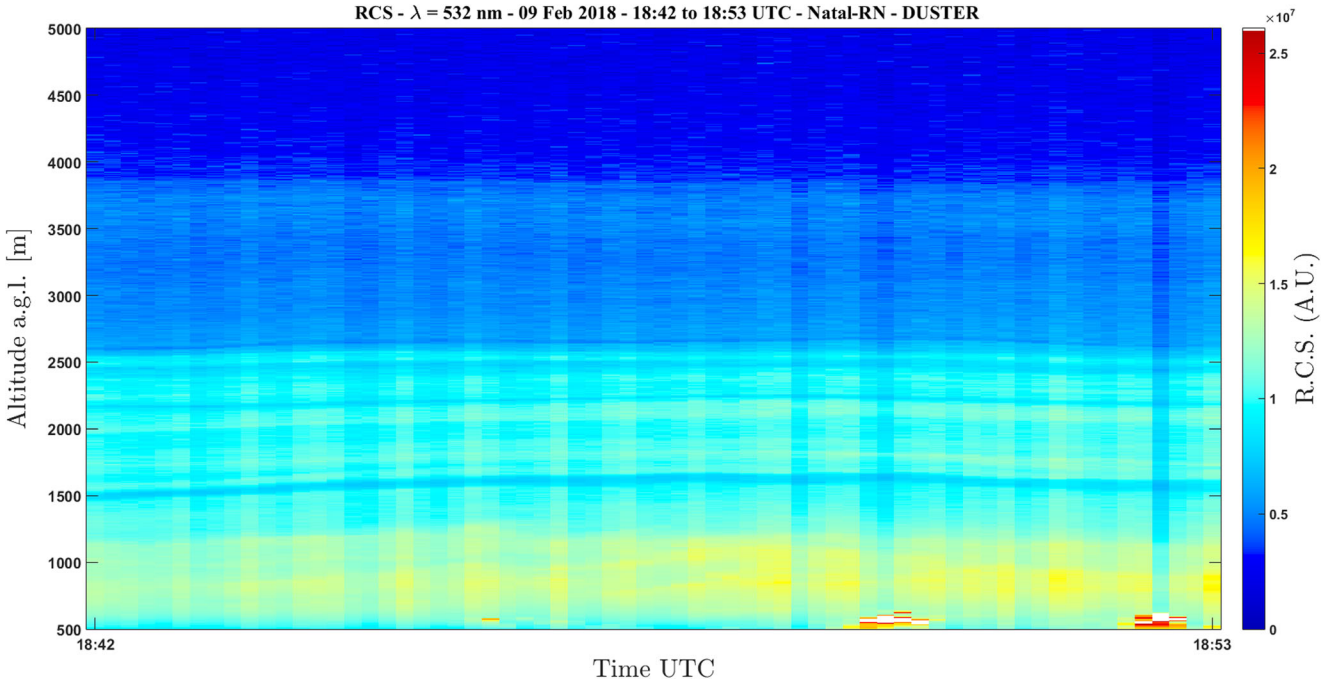

Fig. 13 Profile DUSTER Lidar on February 9, 2018, at Natal from 18:42 to 18:53 UTC with vertical resolution of 3.75 m, temporal resolution of 10 s, and wavelength of 532 nm

dominated by coarse particles (AE < 1). Monthly averages of AE (440–870 nm) from August 2017 to December 2017 showed a high variability that could be attributed to local biomass burning activities. The increase in PW occurred continuously from December 2017 to March 2018, which is the typical period of a southward ITCZ influence. Therefore, the measured optical properties suggested two distinct periods: (1) August to November in which aerosol composition has marine contribution as well as from local sources such as biomass burning and sand dunes and (2) December to March in which the ITCZ is closer to Natal, and allows long-range transport of dust and smoke from the African continent.

Due to high cloud coverage and numerous rain occurrences over Natal, statistically significant measurements of monthly averages of AERONET inversion products (VSD, SSA, RIRP, RIIP, and AF at 440 nm) are reported only from August 2017 to January 2018. The SSA remained around 0.80, which is considered a low value representative for high absorption and can be characteristic for biomass burning aerosols or dust coated by smoke. The RIRP was around 1.50 and the RIIP varied between 0.01 and 0.04, which are characteristic of moderately absorbent aerosols. The AF ranged between 0.73 and 0.80 for the period, which is an indicative of coarse mode predominance. Furthermore, the VSD showed to be bimodal also showing that the coarse mode was predominant. The microphysical properties did not show a clear seasonality but were more linked to the aerosol types.

In summary, optical and microphysical properties of aerosols over Natal showed a dependence on local sources such as dunes, fires, and ocean, and remote sources such as African desert dust and biomass burning, being associated with a wide variation of VSD coarse mode and of the AE. This dependence on sources was most noticeable in September, December, and February. The aerosols also showed to be high and moderately absorbent.

The aerosol typing confirmed, by its optical and microphysical properties, the predominance of marine aerosol (34.80%), mineral dust (6.30%), mixed aerosol (58.10%), and biomass burning (0.80%). Most days classified as mineral dust (11 days) occurred during February 2018 pointing out the aerosol transportation from abroad during this month under the influence of the ITCZ. In addition, the backward trajectories modeled by HYSPLIT identified that half of the air masses originated from the African continent (51%), especially at 3000 m agl, which were likely modeled by the ITCZ and Easterly Wave Disturbances. Additionally, the case study showed an agreement between aerosol typing of the Cimel, MODIS AOD, and the CALIOP aerosol subtype for aerosol layers from African continent at 3000 and 4000 m agl modeled by HYSPLIT and identified by the DUSTER Lidar system, during February 09, 2018, in the atmospheric column of Natal.

Finally, the Cimel Sun-photometer proved to be a reliable tool for obtaining aerosol properties in Natal and its dataset will be extremely useful for obtaining an effective Lidar ratio (Guerrero-Rascado et al. 2009), as well as to provide information for calibrating and validating (or consistency checking) satellite-based products (Jeong et al. 2018), such as from

EarthCARE and AEOLUS, and also aerosol transport models on a regional scale.

Acknowledgments We thank the University of Granada (UGR), Andalusian Institute for Earth System Research (IISTA-CEAMA), Spain, especially Lucas Alados-Arboledas and Juan Luis Guerrero-Rascado and the RIMA network for making the Cimel Sun-photometer available in Natal and for continuous scientific discussions. We thank IF/USP, specifically Prof. Paulo Artaxo, for generous technical support and Dr. Aline Macedo de Oliveira (PPGCC/UFRN) and Dr. Ediclê de Souza Fernandes Duarte (PPGCC/UFRN) for contributions to some of the graphics and discussion of its data. The authors gratefully acknowledge the NOAA Air Resources Laboratory (ARL) for the provision of the HYSPLIT transport and dispersion model and/or READY website (https://www.ready.noaa.gov) used in this publication. The authors wish to also acknowledge the entire CALIPSO team for their substantial contributions and for the data obtained from the NASA Langley Research Center. This article and the research behind it are a direct contribution to the research themes of the Klimapolis Laboratory (klimapolis.net). Networking and coordination activities of the Klimapolis Laboratory are funded by the German Federal Ministry of Education and Research (BMBF).

Authors' contributions This work is based on the master thesis of the first author, Daniel Camilo Fortunato dos Santos Oliveira (DCFSO, who is now Master in Climate Sciences (2019), under supervision of JJH). Contributions of all authors to this work were as follows: Instrument installation and maintenance: DCFSO, EMR, FCM, JJH. Conceptualization: EMR, FJSL, EL, JJH. Methodology: DCFSO, EMR, FJSL, EL, JJH. Formal analysis: DCFSO, JJH. Validation: DCFSO, JJH. Visualization: DCSFO, FJSL, FCM. Writing - original draft: DCFSO, JJH. Writing - review and editing: DCFSO, FJSL, FCM, JJH. Project administration: EL, JJH. Funding acquisition: EL, JJH. Resources: EL, JJH. Software: DCFSO, EMR, FJSL.

Funding University of Granada, Andalusian Institute for Earth System Research (IISTA-CEAMA), Spain: deployment of the Cimel sun-photometer to São Paulo, support in setting up the instrument, and continuous support with the measurements.

Nuclear and Energy Research Institute (IPEN/CNEN), Center for Lasers and Applications (CLA) at the São Paulo, Brazil: deployment of the Cimel sun-photometer to Natal, local and remote support in setting up the instrument, and continuous support with the measurements, support in analysis, and interpretation of data and in writing the manuscript.

University of São Paulo, Institute for Physics (IF/USP): deployment of technical support to Natal, sensor maintenance, continuous support with instrumental issues, support in analysis, and interpretation of data.

The *Coordenação de Aperfeiçoamento de Pessoal de Nível Superior* (CAPES/MCTIC), Brazil, for the master student scholarship of DCFSO.

The National Council for Scientific and Technological Development (CNPq), Brazil, supported the research with a postdoc grant (150716/2017-6) for FJSL and funded the research projects 479252/2011-4, 477713/2013-0, 400430/2014-2, and 432515/2018-6 that allowed to bring the Cimel sun-photometer to Natal, equip the Lidar laboratory at DCAC/UFRN, of which the instrument is part, and permitted carrying out the analyses.

Data availability The datasets generated and/or analyzed during the current study are available:

AERONET-RIMA network, aerosol properties (https://aeronet.gsfc.nasa.gov),

CALIOP/CALIPSO, aerosol subtype (https://www-calipso.larc.nasa.gov/products), MODIS/TERRA/AQUA, AOD (https://ladsweb.modaps.eosdis.nasa.gov),

HYSPLIT, model backward trajectories (https://www.ready.noaa.gov/hypub-bin/trajtype.pl),

Data of the DUSTER Lidar system belong to the Lidar Laboratory of the Department of Atmospheric and Climate Sciences (DCAC) at the Federal University of Rio Grande do Norte (UFRN), Natal, Brazil, and the Center for Lasers and Applications (CLA) at the Nuclear and Energy Research Institute (IPEN/CNEN), São Paulo, Brazil. Data are available from the corresponding author upon reasonable request and with permission of CLA/IPEN.

Compliance with ethical standards

Ethics approval and consent to participate Not applicable.

Consent for publication Not applicable.

Competing interests The authors declare that they have no competing interests.

References

Abouchami W, Näthe K, Kumar A, Galer SJG, Jochum KP, Williams E, Horbe AMC, Rosa JWC, Balsam W, Adams D, Mezger K, Andreae MO (2013) Geochemical and isotopic characterization of the Bodélé Depression dust source and implications for transatlantic dust transport to the Amazon Basin. Earth Planet Sci Lett 380:112–123. https://doi.org/10.1016/j.epsl.2013.08.028

Alvares CA, Stape JL, Sentelhas PC et al (2013) Köppen's climate classification map for Brazil. Meteorol Z. https://doi.org/10.1127/0941-2948/2013/0507

Ansmann A, Baars H, Tesche M et al (2009) Dust and smoke transport from Africa to South America: lidar profiling over Cape Verde and the Amazon rainforest. Geophys Res Lett. https://doi.org/10.1029/2009GL037923

Antuña-Marrero JC, Landulfo E, Estevan R et al (2017) LALINET: the first Latin American-born regional atmospheric observational network. Am Meteorol Soc. https://doi.org/10.1175/BAMS-D-15-00228.1

Baars H, Ansmann A, Althausen D et al. (2011) Further evidence for significant smoke transport from Africa to Amazonia. Geophys Res Lett. https://doi.org/10.1029/2011GL049200

Baars H, Ansmann A, Althausen D et al (2012) Aerosol profiling with lidar in the Amazon Basin during the wet and dry season. J Geophys Res. https://doi.org/10.1029/2012JD018338

Ben-Ami Y, Koren I, Rudich Y et al (2010) Transport of North African dust from the Bodélé depression to the Amazon Basin: a case study. Atmos Chem Phys. https://doi.org/10.5194/acp-10-7533-2010

Ben-Ami Y, Koren I, Altaratz O et al (2012) Discernible rhythm in the spatio/temporal distributions of transatlantic dust. Atmos Chem Phys. https://doi.org/10.5194/acp-12-2253-2012

Bennouna YS, Cachorro VE, Toledano C et al (2011) Comparison of atmospheric aerosol climatologies over southwestern Spain derived from AERONET and MODIS. Remote Sens Environ. https://doi.org/10.1016/j.rse.2011.01.011

Berjón A, Barreto A, Hernández Y et al (2019) A 10-year characterization of the Saharan Air Layer lidar ratio in the subtropical North Atlantic. Atmos Chem Phys. https://doi.org/10.5194/acp-19-6331-2019

BRAZILIAN INSTITUTE OF GEOGRAPHY AND STATISTICS (2020) Available in: https://cidades.ibge.gov.br/brasil/rn/natal/panorama. Accessed 9 Apr 2020 (in Portuguese)

BRAZILIAN NATIONAL INSTITUTE OF METEOROLOGY (2017) Available in: http://www.inmet.gov.br/portal/index.php?r=home2/index. Accessed 13 Nov 2017 (in Portuguese)

Cavalcanti IFA, Ferreira NJ, Silva MGAJS et al (2009) Tempo e Clima no Brasil. Oficina de Textos, São Paulo (in Portuguese)

Coutinho MDL, Lima KC, Santos e Silva CM (2016) Improvements in precipitation simulation over South America for past and future climates via multi-model combination. Clim Dyn. https://doi.org/10.1007/s00382-016-3346-6

Da Silva FR (2015) Estudo do Desenvolvimento da Camada Limite Convectiva no Semiárido Brasileiro. Dissertation, Federal University of Rio Grande do Norte (in Portuguese)

Da Silva PE, Santos e Silva CM, Spyrides MHC et al (2018) Precipitation and air temperature extremes in the Amazon and northeast Brazil. Int J Climatol. https://doi.org/10.1002/joc.5829

De Mazière M, Thompson AM, Kurylo MJ et al (2018) The Network for the Detection of Atmospheric Composition Change (NDACC): history, status and perspectives. Atmos Chem Phys. https://doi.org/10.5194/acp-18-4935-2018

De Oliveira AM, Souza CT, Oliveira NPM et al (2019) Analysis of atmospheric aerosol optical properties in the Northeast Brazilian atmosphere with remote sensing data from MODIS and CALIOP/CALIPSO Satellites, AERONET photometers and a ground-based lidar. Atmosphere. https://doi.org/10.3390/atmos10100594

Derimian Y, Karnieli A, Kaufman YJ et al (2008) The role of iron and black carbon in aerosol light absorption. Atmos Chem Phys. https://doi.org/10.5194/acp-8-3623-2008

Diniz MTM, Pereira VHC (2015) Climatologia do Estado do Rio Grande do Norte, Brasil: Sistemas Atmosféricos Atuantes e Mapeamento de Tipos de Clima. Bolet Goian Geogr. https://doi.org/10.5216/bgg.v35i3.38839 (in Portuguese)

Dubovik O, King MD (2000) A flexible inversion algorithm for retrieval of aerosol optical properties from Sun and sky radiance measurements. J Geophys Res. https://doi.org/10.1029/2000JD900282

Dubovik O, Holben BN, Eck TF et al. (2002) Variability of absorption and optical properties of key aerosol types observed in worldwide locations. J Atmos Sci. https://doi.org/10.1175/1520-0469(2002)059<0590:VOAAOP>2.0.CO;2

Eck TF, Holben BN, Reid JS et al (1999) Wavelength dependence of the optical depth of biomass burning, urban, and desert dust aerosol. J Geophys Res. https://doi.org/10.1029/1999JD900923

Eck TF, Holben BN, Dubovik O et al (2005) Columnar aerosol optical properties at AERONET sites in central eastern Asia and aerosol transport to the tropical mid-Pacific. J Geophys Res. https://doi.org/10.1029/2004JD005274

Eck TF, Holben BN, Sinyuk A et al (2010) Climatological aspects of the optical properties of fine/coarse mode aerosol mixtures. J Geophys Res. https://doi.org/10.1029/2010JD014002

Feingold G, McComiskeyb A, Yamaguchia T et al (2016) New approaches to quantifying aerosol influence on the cloud radiative effect. PNAS. https://doi.org/10.1073/pnas.1514035112

Formenti P, Rajot JL, Desboeufs K et al (2008) Regional variability of the composition of mineral dust from western Africa: results from the AMMA SOP0/DABEX and DODO field campaigns. J Geophys Res. https://doi.org/10.1029/2008JD009903

Foyo-Moreno I, Alados I, Guerrero-Rascado JL et al (2019) Contribution to column-integrated aerosol typing based on Sun-photometry using different criteria. Atmos Res. https://doi.org/10.1016/j.atmosres.2019.03.007

Fuzzi S, Baltensperger U, Carslaw K et al (2015) Particulate matter, air quality and climate: lessons learned and future needs. Atmos Chem Phys. https://doi.org/10.5194/acp-15-8217-2015

Galvão MFO, De Queiroz JDF, Duarte ESF (2016) Characterization of the particulate matter and relationship between buccal micronucleus and urinary 1-hydroxypyrene levels among cashew nut roasting workers. Environ Pollut https://doi.org/10.1016/j.envpol.2016.10.024

Gasteiger J, Groβ S, Sauer D et al (2017) Particle settling and vertical mixing in the Saharan Air Layer as seen from an integrated model, lidar, and in situ perspective. Atmos Chem Phys. https://doi.org/10.5194/acp-17-297-2017

Giles DM, Holben BN, Eck TF et al. (2012) An analysis of AERONET aerosol absorption properties and classifications representative of aerosol source regions. J Geophys Res. https://doi.org/10.1029/2012JD018127

Giles DM, Sinyuk A, Sorokin MG et al (2019) Advancements in the Aerosol Robotic Network (AERONET) Version 3 Database – automated near real-time quality control algorithm with improved cloud screening for sun photometer aerosol optical depth (AOD) measurements. Atmos Meas Tech. https://doi.org/10.5194/amt-12-169-2019

Gomes HB, Ambrizzi T, Herdies DL et al (2015) Easterly wave disturbances over Northeast Brazil: an observational analysis. Hindawi Publishing Corporation. Adv Meteorol. https://doi.org/10.1155/2015/176238

Guerrero-Rascado JL, Olmo FJ, Avilés-Rodriguez I et al (2009) Extreme Saharan dust event over the southern Iberian Peninsula in September 2007: active and passive remote sensing from surface and satellite. Atmos Chem Phys. https://doi.org/10.5194/acp-9-8453-2009

Guerrero-Rascado JL, Landulfo E, Antuña JC et al (2016) Latin American Lidar Network (LALINET) for aerosol research: diagnosis on network instrumentation. J Atmos Sol Terr Phys. https://doi.org/10.1016/j.jastp.2016.01.001

Hamill P, Giordano M, Ward C et al (2016) An AERONET-based aerosol classification using the Mahalanobis distance. Atmos Environ. https://doi.org/10.1016/j.atmosenv.2016.06.002

Hansen JE, Travis LD (1974) Light scattering in planetary atmospheres. Space Sci Rev. https://doi.org/10.1007/BF00168069

Hansen J, Sato M, Ruedy R (1997) Radiative forcing and climate response. J Geophys Res. https://doi.org/10.1029/96JD03436

Hastenrath S (1991) Climate dynamics of the tropics. Kluwer Academic Publishers, Dordrecht

Hoelzemann JJ, Longo KM, Fonseca RM (2009) Regional representativity of AERONET observation sites during the biomass burning season in South America determined by correlation studies with MODIS Aerosol Optical Depth. J Geophys Res. https://doi.org/10.1029/2008JD010369

Holben BN, Eck TF, Slutsker I et al (1998) AERONET-A federated instrument network and data archive for aerosol characterization. Remote Sens Environ. https://doi.org/10.1016/S0034-4257(98)00031-5

Holben BN, Tanré D, Smirnov A et al (2001) An emerging ground-based aerosol climatology: aerosol optical depth from AERONET. J Geophys Res. https://doi.org/10.1029/2001JD900014

Holben BN, Eck TF, Slutsker I et al (2006) AERONET's Version 2.0 quality assurance criteria. Remote Sens Atmos Clouds. https://doi.org/10.1117/12.706524

Illingworth AJ, Barker HW, Beljaars A et al (2015) The EarthCARE satellite: the next step forward in global measurements of clouds, aerosols, precipitation, and radiation. Am Meteorol Soc. https://doi.org/10.1175/BAMS-D-12-00227.1

INTERGOVERNMENTAL PANEL ON CLIMATE CHANGE (2013) Climate change 2013: the physical science basis. Cambridge University Press, New York

INTERGOVERNMENTAL PANEL ON CLIMATE CHANGE (2018) Special report: global warming of 1.5 °C. Cambridge University Press, New York

James PE (1939) Air masses and fronts in South America. Geogr Rev. Taylor & Francis, Ltd. http://www.jstor.org/stable/210071

Jeong U, Tsay SC, Pantina P et al (2018) Langley calibration analysis of solar spectroradiometric measurements: spectral aerosol optical

thickness retrievals. J Geophys Res Atmos. https://doi.org/10.1002/2017JD028262

Junior FCV, Jones C, Gandu AW (2018) Interannual and intraseasonal variations of the onset and demise of the pre-wet season and the wet season in the Northern Northeast Brazil. Rev Bras Meteorol. https://doi.org/10.1590/0102-7786333007

Karyampudi VM, Carlson TN (1988) Analysis and numerical simulations of the Saharan air layer and its effect on easterly wave disturbances. J Atmos Sci. https://doi.org/10.1175/1520-0469(1988)045<3102:AANSOT>2.0.CO;2

Karyampudi VM, Palm SP, Reagen JA et al (1999) Validation of the Saharan dust plume conceptual model using lidar, Meteosat, and ECMWF data. Bull Am Meteorol Soc. https://doi.org/10.1175/1520-0477(1999)080<1045:VOTSDP>2.0.CO;2

Kaufman YJ (1993) Aerosol optical thickness and atmospheric path radiance. J Geophys Res. https://doi.org/10.1029/92JD02427

Kaufman YJ, Tanré D, Boucher O (2002) A satellite view of aerosol in the climate system. Nat Publ Group. https://doi.org/10.1038/nature01091

Kaufman YJ, Koren I, Remer LA et al (2006) Dust transport and deposition observed from the Terra-Moderate Resolution Imaging Spectroradiometer (MODIS) spacecraft over the Atlantic Ocean. J Geophys Res. https://doi.org/10.1029/2003JD004436

Kim MH, Omar AH, Tackett JL et al (2018) The CALIPSO version 4 automated aerosol classification and lidar ratio selection algorithm. Atmos Meas Tech. https://doi.org/10.5194/amt-11-6107-2018

Knobelspiesse KD, Pietras C, Fargion GS et al (2004) Maritime aerosol optical thickness measured by handheld sun photometers. Remote Sens Environ. https://doi.org/10.1016/j.rse.2004.06.018

Koren I, Kaufman YJ, Remer LA et al (2004) Measurement of the effect of Amazon smoke on inhibition of cloud formation. Science. https://doi.org/10.1126/science.1089424

Koren I, Martins JV, Remer LA et al (2008) Smoke invigoration versus inhibition of clouds over the Amazon. Science 321:946–949. https://doi.org/10.1126/science.1159185

Koren I, Altaratz O, Dagan G (2015) Aerosol effect on the mobility of cloud droplets. Environ Res Lett. https://doi.org/10.1088/1748-9326/10/10/104011

Kumar A, Abouchami W, Galer SJG et al (2014) A radiogenic isotope tracer study of transatlantic dust transport from Africa to the Caribbean. Atmos Environ. https://doi.org/10.1016/j.atmosenv.2013.10.021

Landulfo E, Lopes FJS, Montilla-Rosero E et al (2016) DUSTER Lidar: Transatlantic transport of aerosol particles from the Sahara and other sources: first results from the recently installed Lidar and sunphotometer in Natal/Brazil. Proceedings of SPIE, the International Society for Optical Engineering. https://doi.org/10.1117/12.2241386

Levy RC, Remer LA, Kleidman RG et al (2010) Global evaluation of the Collection 5 MODIS dark-target aerosol products over land. Atmos Chem Phys. https://doi.org/10.5194/acp-10-10399-2010

Liu Z, Omar A, Vaughan M et al (2008) CALIPSO lidar observations of the optical properties of Saharan dust: a case study of long-range transport. J Geophys Res. https://doi.org/10.1029/2007JD008878

Marengo JA, Alves LM, Beserra EA et al. (2011) Variabilidade e mudanças climáticas no semiárido brasileiro. Recursos hídricos em regiões áridas e semiáridas, Campina Grande (in Portuguese)

Marengo JÁ, Torres RR, Alves LM (2016) Drought in Northeast Brazil-past, present, and future. Theor Appl Climatol. https://doi.org/10.1007/s00704-016-1840-8

Mateos D, Cachorro VE, Toledano C et al (2015) Columnar and surface aerosol load over the Iberian Peninsula establishing annual cycles, trends, and relationships in five geographical sectors. Sci Total Environ. https://doi.org/10.1016/j.scitotenv.2015.03.002

Melo ABC et al (2009) Zona de Convergência Intertropical do Atlântico. In: Cavalcanti IFA et al (eds) Tempo e Clima no Brasil, 1st edn. Oficina de Textos, São Paulo, pp 25–39 (in Portuguese)

Molion LCB, Bernardo SDO (2002) Uma revisão da dinâmica das chuvas no Nordeste brasileiro. Revista Brasileira de Meteorologia. Available in: http://www.scielo.br/scielo.php?script=sci_serial&pid=0102-7786&lng=en&nrm=iso Accessed 23 March 2018 (in Portuguese)

Moran-Zuloaga D, Ditas F, Walter D et al (2018) Long-term study on coarse mode aerosols in the Amazon rain forest with the frequent intrusion of Saharan dust plumes. Atmos Chem Phys. https://doi.org/10.5194/acp-18-10055-2018

Motta AG (2004) O CLIMA DE NATAL. Instituto Nacional de Pesquisas Espaciais, São José dos Campos. Available in: http://mtcm16.sid.inpe.br/col/sid.inpe.br/marciana/2004/10.21.09.04/doc/LivroClima.pdf Accessed 15 April 2017 (in Portuguese)

Muyimbwa D, Frette Ø, Stamnes JJ et al (2015) Aerosol optical properties and precipitable water vapor column in the atmosphere of Norway. Appl Opt. https://doi.org/10.1364/AO.54.001505

National Institute of Space Research (2020) Available in: http://queimadas.dgi.inpe.br/queimadas/bdqueimadas. Accessed 14 Apr 2020 (in Portuguese)

Nishizawa T, Sugimoto N, Matsui I et al (2016) The Asian dust and aerosol lidar observation network (AD-Net): strategy and progress. EPJ Web Conf. https://doi.org/10.1051/epjconf/201611919001

O'Neill NT, Ignatov A, Holben BN et al (2000) The lognormal distribution as a reference for reporting aerosol optical depth statistics; empirical tests using multi-year, multi-site AERONET sunphotometer data. Geophys Res Lett. https://doi.org/10.1029/2000GL011581

O'Neill NT, Dubovik O, Eck TF (2001) Modified Ångström exponent for the characterization of submicrometer aerosol. Appl Opt. https://doi.org/10.1364/AO.40.002368

Oliveira PT, Santos e Silva CM, Lima KC (2016) Climatology and trend analysis of extreme precipitation in subregions of Northeast Brazil. Theor Appl Climatol. https://doi.org/10.1007/s00704-016-1865-z

Olmo FJ, Quirantes A, Alcántara A et al (2006) Preliminary results of a non-spherical aerosol method for the retrieval of the atmospheric aerosol optical properties. J Quant Spectrosc Radiat Transf. https://doi.org/10.1016/j.jqsrt.2005.11.047

Olmo FJ, Quirantes A, Lara V et al (2008) Aerosol optical properties assessed by an inversion method using the solar principal plane for non-spherical particles. J Quant Spectrosc Radiat Transf. https://doi.org/10.1016/j.jqsrt.2007.12.019

Omar AH, Winker DM, Kittaka C et al (2009) The CALIPSO automated aerosol classification and Lidar Ratio Selection Algorithm. J Atmos Ocean Technol. https://doi.org/10.1175/2009JTECHA1231.1

Omar AH, Winker DM, Tackett JL et al (2013) CALIOP and AERONET aerosol optical depth comparisons: one size fits none. J Geophys Res. https://doi.org/10.1002/jgrd.50330

Orza JAG, Perrone MR (2015) Trends in the aerosol load properties over south eastern Italy. IOP Conf Ser: Earth Environ Sci. https://doi.org/10.1088/1755-1315/28/1/012011

Paixão MMA (2011) Propriedades Ópticas de Aerossóis Naturais de Queimadas da Amazônia. Dissertation, University of São Paulo. (in Portuguese)

Pappalardo G, Amodeo A, Apituley A et al (2014) EARLINET: towards an advanced sustainable European aerosol lidar network. Atmos Meas Tech. https://doi.org/10.5194/amt-7-2389-2014

Perrone MR, Santese M, Tafur AM et al (2005) Aerosol load characterization over South–East Italy for one year of AERONET sunphotometer measurements. Atmos Res. https://doi.org/10.1016/j.atmosres.2004.12.003

Prats N, Cachorro VE, Sorribas M et al (2008) Columnar aerosol optical properties during "El Arenosillo 2004 summer campaign". Atmos Environ. https://doi.org/10.1016/j.atmosenv.2007.07.041

Reboita MS, Gan MA, Da Rocha RP et al. (2010) Regimes de Precipitação na América do Sul: Uma Revisão Bibliográfica. Rev Bras Meteorol. https://doi.org/10.1590/S0102-77862010000200004 (in Portuguese)

Reboita MS, Krusche N, Ambrizzi T et al (2012) Entendendo o Tempo e o Clima na América do Sul. Ter e Didát. https://doi.org/10.20396/td.v8i1.8637425 (in Portuguese)

Reboita MS, Rodrigues M, Armando RP et al (2016) Causas da Semiaridez do Sertão Nordestino. Rev Bras Climatol. https://doi.org/10.5380/abclima.v19i0.42091 (in Portuguese)

Remer LA, Kaufman YJ, Tanré D et al (2005) The MODIS Aerosol Algorithm, Products, and Validation. J Atmos Sci. https://doi.org/10.1175/JAS3385.1

Rizzo LV, Artaxo P, Müller T et al (2013) Long term measurements of aerosol optical properties at a primary forest site in Amazonia. Atmos Chem Phys. https://doi.org/10.5194/acp-13-2391-2013

Rodríguez S, Calzolai G, Chiari M et al (2020) Rapid changes of dust geochemistry in the Saharan Air Layer linked to sources and meteorology. Atmos Environ. https://doi.org/10.1016/j.atmosenv.2019.117186

Seinfeld JH, Pandis SN (2016) Atmospheric chemistry and physics: from air pollution to climate change. John Wiley & Sons, New Jersey

Seinfeld JH, Bretherton C, Carslaw KS et al (2016) Improving our fundamental understanding of the role of aerosol−cloud interactions in the climate system. PNAS. https://doi.org/10.1073/pnas.1514043113

Sena ET, Artaxo P (2015) A novel methodology for large-scale daily assessment of the direct radiative forcing of smoke aerosols. Atmos Chem Phys. https://doi.org/10.5194/acp-15-5471-2015

Sinyuk A, Holben BN, Eck TF et al (2020) The AERONET Version 3 aerosol retrieval algorithm, associated uncertainties and comparisons to Version 2. Atmos Meas Tech. https://doi.org/10.5194/amt-13-3375-2020

Smirnov A, Holben BN, Kaufman YJ et al (2002) Optical properties of atmospheric aerosol in maritime environments. J Atmos Sci. https://doi.org/10.1175/1520-0469(2002)059<0501:OPOAAI>2.0.CO;2

Sokolik IN, Toon OB (1999) Incorporation of mineralogical composition into models of the radiative properties of mineral aerosol from UV to IR wavelengths. J Geophys Res. https://doi.org/10.1029/1998JD200048

Stein AR, Draxler G, Rolph B et al (2015) NOAA's HYSPLIT atmospheric transport and dispersion modeling system. Am Meteorol Soc. https://doi.org/10.1175/BAMS-D-14-00110.1

Swap R, Garstang M, Greco S (1992) Saharan dust in the Amazon Basin. Tellus. https://doi.org/10.3402/tellusb.v44i2.15434

Talbot RW, Andreae MO, H B et al (1990) Aerosol chemistry during the wet season in central Amazonia: the influence of long-range transport. J Geophys Res. https://doi.org/10.1029/JD095iD10p16955

Tan F, Lim S, Abdullah K et al (2015) AERONET data–based determination of aerosol types. Atmos Pollut Res. https://doi.org/10.5094/APR.2015.077

Taylor M, Kazadzisa S, Amiridis V et al (2015) Global aerosol mixtures and their multiyear and seasonal characteristics. Atmos Environ. https://doi.org/10.1016/j.atmosenv.2015.06.029

Thorsen TJ, Ferrare RA, Kato S et al (2020) Aerosol direct radiative effect sensitivity analysis. J Clim. https://doi.org/10.1175/JCLI-D-19-0669.1

Toledano C, Cachorro VE, Berjón A et al (2007) Aerosol optical depth and Ångström exponent climatology at El Arenosillo AERONET site (Huelva, Spain). Q J R Meteorol Soc. https://doi.org/10.1002/qj.54

Toledano C, Cachorro VE, De Frutos AM et al (2009) Airmass classification and analysis of aerosol types at El Arenosillo (Spain). J Appl Meteorol Climatol. https://doi.org/10.1175/2008JAMC2006.1

Tsamalis C, Chédin A, Pelon J et al (2013) The seasonal vertical distribution of the Saharan Air Layer and its modulation by the wind. Atmos Chem Phys. https://doi.org/10.5194/acp-13-11235-2013

Valenzuela A, Olmo FJ, Lyamani H et al. (2010) Aerosol properties retrieved from sky radiance at the principal plane for nonspherical particles. IV Reunión Española de Ciencia y Tecnología del Aerosol - RECTA 2010

Vergaz R, Cachorro VE, De Frutos AM et al (2005) Columnar characteristics of aerosols by spectroradiometer measurements in the maritime area of the Cadiz Gulf (Spain). Int J Climatol. https://doi.org/10.1002/joc.1208

Wagner F, Silva AM (2008) Some considerations about Ångström exponent distributions. Atmos Chem Phys. https://doi.org/10.5194/acp-8-481-2008

Wang Q, Saturno J, Chi X et al (2016) Modeling investigation of light-absorbing aerosols in the Amazon Basin during the wet season. Atmos Chem Phys. https://doi.org/10.5194/acp-16-14775-2016

Wehrli C (2000) PFR precision filter radiometer documentation. World Radiation Center, Observatorium, Davos

Weinzierl B, Sauer D, Esselborn M et al (2011) Microphysical and optical properties of dust and tropical biomass burning aerosol layers in the Cape Verde region – an overview of the airborne in situ and lidar measurements during SAMUM-2. Tellus. https://doi.org/10.1111/j.1600-0889.2011.00566.x

Welton EJ, Campbell JR, Spinhirne JD et al (2001) Global monitoring of clouds and aerosols using a network of micro-pulse lidar systems. Proc SPIE 4153:151–158

Winker DM, Vaughan MA, Omar A et al (2009) Overview of the CALIPSO mission and CALIOP data processing algorithms. J Atmos Ocean Technol. https://doi.org/10.1175/2009JTECHA1281.1